Strong-coupling fixed point instability in a single-channel SU(N) Kondo model

Andrés Jerez,[1] Mireille Lavagna,[2,*] and Damien Bensimon[2,3]
[1]*European Synchrotron Radiation Facility, 6, rue Jules Horowitz, 38043 Grenoble Cedex 9, France*
[2]*Commissariat à l'Energie Atomique, DRFMC /SPSMS, 17, rue des Martyrs, 38054 Grenoble Cedex 9, France*
[3]*Department of Applied Physics, University of Tokyo, Bunkyo-Ku, Tokyo 113-8656, Japan*
(Received 20 December 2002; revised manuscript received 5 June 2003; published 12 September 2003)

We study a generalized SU(N) single-impurity Kondo model in which the impurity spin is described by a combination of q Abrikosov fermions and $(2S-1)$ Schwinger bosons. Our aim is to describe both the quasiparticlelike excitations and the locally critical modes observed in various physical situations, including non-Fermi-liquid behavior in heavy-fermion systems in the vicinity of a quantum critical point. We carry out an analysis of the strong-coupling fixed point, from which an effective Hamiltonian is derived containing both a charge interaction and a spin coupling between n_d nearest-neighbor electrons and the screened impurity. The effective charge interaction is already present in the case of a purely fermionic impurity and it changes from repulsive to attractive at $q=N/2$, due to the $q\rightarrow N-q$ symmetry. The sign of the effective spin coupling determines the stability of the strong-coupling fixed point. Already in the single-channel case and in contrast with either the pure bosonic or the pure fermionic case, the strong-coupling fixed point is unstable against the conduction electron kinetic term in the large-N limit as soon as $q>N/2$. The origin of this change of regime is directly related to the sign of the effective charge interaction.

DOI: 10.1103/PhysRevB.68.094410 PACS number(s): 75.20.Hr, 75.30.Mb, 71.10.Hf

I. INTRODUCTION

Recent experiments in heavy-fermion compounds have shown the existence of a quantum phase transition from a magnetically disordered to a long-range magnetic ordered phase, driven by change in chemical composition, pressure, or magnetic field.[1] For an extensive survey of the experimental situation we refer the reader to the review paper of Stewart.[2] In a very unusual way, the behavior of the system in the disordered phase close to the quantum critical point (QCP) differs from that of a Fermi liquid. For example $CeCu_{6-x}Au_x$ (Refs. 3 and 4) and $(Ce_{1-x}La_x)Ru_2Si_2$ (Ref. 5) present an antiferromagnetic transition, respectively, at $x_C=0.1$ and $x_C=0.08$. While far from the QCP, the magnetically disordered phase is a Fermi liquid with a large effective mass, the temperature dependence of the physical quantities in the disordered phase in the vicinity of the QCP is of non-Fermi-liquid-like type. Typically, in $CeCu_{5.9}Au_{0.1}$,[4] the specific heat C depends on T as $C/T\sim-\ln(T/T_0)$, the magnetic susceptibility as $\chi\sim 1-\alpha\sqrt{T}$, and the T-dependent part of the resistivity as $\Delta\rho\sim T$ instead of $C/T\sim\chi\sim$Const and $\Delta\rho\sim T^2$ as in the Fermi-liquid state. Once a long-range magnetic order is set up, the effect of a pressure or of a magnetic field is to drive the system back to a magnetically disordered phase with a Fermi-liquid behavior. The same type of behavior has been observed in other systems such as $YbRh_2Si_2$,[6] $CeNi_2Ge_2$,[7] $CeCu_2(Si_{1-x}Ge_x)_2$,[8] $CeIn_3$, $CePd_2Si_2$,[9] and $U_{1-x}Y_xPd_3$.[10] The associated breakdown of the Fermi-liquid theory poses fundamental questions about the possible formation of novel electronic states of matter with new types of elementary excitations resulting from the presence of strong correlations among electrons.

On the theoretical side, two scenarios are in competition to describe quantum phase transitions: either the itinerant magnetism scenario (i), or more recently proposed, the locally critical picture (ii).

In the former case, (i), the quasiparticles still exist at the QCP and the theory focuses on the study of the low-lying, large-wavelength (low-ω, low-q) fluctuations of the order parameter close to the transition. The calculations have been performed within the renormalization-group scheme[11–13] or in the self-consistent spin-fluctuation theory,[14] and have been recently extended[15] to the microscopic model which is believed to describe the heavy fermions, the Kondo lattice. In all the cases, they lead to a Φ^4 theory with an effective dimension $d_{eff}=d+z$ where d is the spatial dimension and z is the dynamic exponent. In the experimental situations, d_{eff} is above its upper critical value equal to 4, since d is equal to 3 or 2, and z varies from 2 to 3 depending on whether the spin fluctuations are staggered or uniform. Hence the system is described by a Gaussian fixed point with anomalous temperature dependence of C/T and $a=\Delta\rho/T$ but with predictions that cannot account for the non-Fermi-liquid behavior observed experimentally.

The second scenario, (ii), has been motivated by the recent results obtained by inelastic neutron-scattering experiments performed on $CeCu_{5.9}Au_{0.1}$. The dynamical spin susceptibility $\chi''(\mathbf{q},\omega)$ near the magnetic instability wave vector $\mathbf{Q}$ has been found to obey an anomalous ω/T scaling law[16,17] as a function of temperature: $\chi''(\mathbf{Q},\omega)\sim T^{-\alpha}g(\omega/T)$ with an exponent α of order 0.75. Moreover, such a ω and T dependence appear to stand over the entire Brillouin zone revealing in the bulk susceptibility too. This fact strongly suggests that the spin dynamics are critical not only at large length scales[18,19] but also at atomic length scales, contrary to what happens in the traditional itinerant magnetism picture, (i). From these results, one can deduce that local critical modes coexist with large-wavelength fluctuations of the order parameter implying a non-Gaussian fixed point beyond the Φ^4 theory.

Alternative theories to the spin-fluctuation scheme are needed to describe the local feature of the quantum critical point characterized by the simultaneous disappearance of the

quasiparticles and the formation of local moments. This has been the subject of much interest these last years with the consideration of single-impurity Kondo models including coupling either to soft-gap fermionic bath or to both fermionic and bosonic baths (for a review, see Ref. 20). The former case corresponds to a fermionic bath with a vanishing density of states at the Fermi level[21] following a power law $\rho(\epsilon)\sim|\epsilon|^r$ $(r>0)$. It is known to display a quantum critical point QCP driven by critical local-moment fluctuations, from a strong-coupling (SC) phase with complete Kondo screening to a local moment (LM) phase.[21–23] The QCP is characterized by nontrivial behavior of the system as, for instance, scaling law for the dynamical spin susceptibility[22] following $\chi''(\omega)\sim g(\omega/T)$. The second case corresponds to coupling to both fermionic and bosonic baths where bosons represent collective spin excitations (see Refs. 20 and 19, and references within). As expected, the bosonic excitations become gapless at the QCP and the spectral density follows a power law in ω. This model shows strong similarities with the soft-gap model mentioned just above with suppression of the Kondo effect due to critical local-moment fluctuations leading to a local-moment phase. Here again recent calculations based on numerical renormalization group (NRG) or dynamical mean field theory approaches[19] seem to indicate the existence of scaling law in ω/T for the dynamical spin susceptibility in the vicinity of the QCP.

The other theories developed so far in order to describe the local QCP, are based on the idea of supersymmetry.[24–27] In these theories, the spin is described in a mixed fermionic-bosonic representation. The interest of the supersymmetric approach is to allow to describe the quasiparticles and the local moments on an equal footing through the fermionic and the bosonic part of the spin, respectively. It appears to be specially well indicated in the case of the locally critical scenario in which the magnetic temperature scale T_N and the Fermi scale T_K (the Kondo temperature) below which the quasiparticles die, vanish at the same point, δ_C.

An important aspect in the discussion of the breakdown of the Fermi-liquid theory is related to the question of the stability of the SC fixed point. Whereas all the issues presented previously concerning heavy-fermion systems have to do with properties of the lattice, the instability of the SC fixed point can be regarded already by studying the single-impurity problem.

The traditional source of instability in the single-impurity Kondo model is the presence of several channels for the conduction electrons with the existence of two regimes, underscreened and overscreened, with very different behaviors as we are about to recall. Indeed we will see that this is not the only possible source of instability of the strong-coupling fixed point. Recent works have shown that more general Kondo impurities of symmetry group SU(N) may also lead to an instability of the SC fixed point already with one channel of conduction electrons.[26,27]

In order to fix ideas, let us start with the antiferromagnetic single-channel Kondo impurity model. It is well known that within a renormalization group (RG) analysis,[28–30] the flow takes the Kondo coupling J all the way to strong coupling. The weak-coupling β function follows the renormalization group equation

$$\beta(g)=\frac{dg(\Lambda)}{d\Lambda}=-g^2, \tag{1}$$

where $g=\rho_0 J$ and ρ_0 is the density of states of conduction electrons. The system flows to a strong coupling fixed point which is stable and the associated behavior of the system is that of a local Fermi liquid.

The situation is rather different when one considers several channels for the conduction electrons. In the case of a spin S in Kondo interaction with conduction electrons belonging to K different channels, Blandin and Nozières[31] have shown that the multichannel Kondo model can lead to two very different situations depending on how K compares to $2S$. Their calculation corresponds to a second-order perturbation theory in the hopping amplitude t of the conduction electrons, around the strong-coupling fixed point. They analyze their results by deriving an effective coupling J_{eff} between the spin of the composite formed by the impurity dressed by the conduction electrons in the strong-coupling limit, and the spin of the conduction electron on the neighboring sites. They are then able to apply the same RG analysis to J_{eff} as indicated in Eq. (1). In the underscreened regime, when $K<2S$, the effective coupling is found to be ferromagnetic and the strong coupling fixed point is stable. In the overscreened regime when $K>2S$, the effective coupling is found to be antiferromagnetic and hence the strong-coupling fixed point is unstable. The former $K<2S$ regime corresponds to the one-stage Kondo effect with the formation of an effective spin $(S-1/2)$ resulting from the screening of the impurity spin by the conduction electrons located on the same site. The system described by the strong-coupling fixed point, behaves as a local Fermi liquid. The instability of the strong-coupling fixed point in the overscreened regime is an indication of the existence of an intermediate coupling fixed point which has been then investigated[32–34] by means of other methods. As is well established now, the intermediate coupling fixed point leads to non-Fermi-liquid excitation spectrum with an anomalous residual entropy at zero temperature.

It has recently been put forward that other sources of instability of the SC fixed point may exist besides the multiplicity of the conduction electron channels. Recent works[26,27] have shown that the presence of a more general Kondo impurity where the spin symmetry is extended from SU(2) to SU(N), and the representation is given by a L-shaped Young tableau, may also lead to an instability of the SC fixed point already in the one-channel case. In the large N limit, Coleman *et al.* (Refs. 26 and 27) have found that the SC fixed point becomes unstable as soon as q (the number of boxes in the Young tableau along the first column) is larger than $N/2$, whatever may be the value of $2S$ (the number of boxes in the Young tableau along the first row). The consideration of a L-shaped Kondo impurity fits in with the supersymmetry approach that we have evoked before since both spin operators and states can be expressed in terms of bosons and fermions.

At that point, it is worth noting that the supersymmetry theory, or specifically taking into consideration more general L-shaped Kondo impurities, appears to offer valuable insights into the two issues raised by the breakdown of the Fermi-liquid theory that we have summarized above, i.e., both the existence of locally critical modes and the question of the instability of the SC fixed point. In the same way as large N expansions may provide insights into real systems even at finite value of the degeneracy, the study of more general impurities may enlighten the understanding of experimental situations with the coexistence of quasiparticles and localized moments that may eventually lead to a phase transition as the coupling to other impurities become dominant.

The aim of the paper is to study the L-shaped, single-impurity, single-channel, SU(N) Kondo model. We want to understand how the system behaves, not only as a function of the impurity parameters $(2S,q)$, but also as a function of the number of electrons n_d available on neighboring sites, that is to say, of the filling. As long as the bosonic component of spin is of order N, there is a transition around the point where the fermionic component of the impurity is $q=N/2$. At this particular point, the energy shift is, to lowest order in perturbation theory around the strong-coupling fixed point, equal to $(-2t^2/J)$, independently of the impurity parameters, q, S, and N. Our study reveals that the phase diagram of the system is not accidental, but is due to the relation of the effective dressed impurity in the strong-coupling regime to the conduction electrons in neighboring sites. If $q<N/2$, there is a repulsive effective potential acting on the nearest-neighbor site of the impurity. This potential becomes attractive for $q>N/2$. This change in behavior happens at the same place where the strong-coupling fixed point becomes unstable. That is, in the repulsive regime the strong-coupling fixed point is stable. However, the attractive regime is not realized as such since the strong-coupling fixed point becomes unstable for $q>N/2$.

The rest of the paper is organized as follows. In Sec. II, we introduce the model and the main features of the strong-coupling limit, where the electron kinetic term is neglected. In this limit the model is reduced to a single site problem, where the impurity is coupled to n_c conduction electrons.[27] We identify the ground state and the energies of the excited states with one more or one less conduction electron, which will play a role in the lowest order in perturbation theory. In Sec. III, we derive the effective Hamiltonian resulting from a second-order perturbation calculation in t around the strong-coupling fixed point. It includes both an effective coupling and an effective interaction between the dressed impurity at site 0 and the conduction electrons on the adjacent site. The sign of the effective spin coupling J_{eff} directly controls the stability of the strong coupling fixed point in the sense that J_{eff} can be incorporated in turn into the renormalization-group equations driving the renormalization flow of the system. When the effective coupling J_{eff} is ferromagnetic, the flow takes the system to $J_{eff}=0$ and the strong-coupling fixed point turns out to be stable. When the effective coupling J_{eff} is antiferromagnetic, the flow takes the system away from the strong-coupling fixed point to an intermediate coupling fixed point. The sign of the effective charge interaction U_{eff} informs on the repulsive or attractive effect of the dressed impurity on the conduction electrons on the adjacent site. Section IV contains the discussion of the results. In the large N limit, we show how J_{eff} is derived from the energy shift difference between the symmetric and the antisymmetric configurations, and how the analysis of the n_d dependence of the energy shift provides information on the effective charge interaction U_{eff}. When the behavior of the system is controlled by the strong-coupling fixed point, i.e., when $q<N/2$, the impurity in the ground state tends to *repel* electrons on neighboring sites. Once $q>N/2$, the repulsion becomes attraction. We show how this feature is already present in the purely fermionic case, and is a consequence of the *particle-hole* symmetry, $q\rightarrow N-q$. The fact that there is extra degeneracy in the supersymmetric impurity, due to the bosonic contribution, leads to the instability of the strong-coupling fixed point as soon as $q>N/2$. We finish the section with a short discussion on the behavior of physical quantities in the different regimes.

The appendixes contain the technical details of the calculations, which involve a higher level of complexity than those of Ref. 27, where only the explicit form of the ground state was needed. When $n_d>1$, there is more than one intermediate state in some of the virtual processes considered, and we need to use the explicit form of the intermediate states. In Appendix A we outline the construction of three particle states with SU(3) symmetry, as an introduction to the group theoretical formalism used. Explicit expressions for the impurity states and the eigenstates of the model in the strong-coupling limit are derived in Appendix B. We also include a general presentation of the different representations of the spin, either bosonic, fermionic, or L shaped, as considered in the paper. We will show how in the latter case the spin operators and the impurity states are expressed in terms of fermion and boson creation and annihilation operators within two constraints. Appendix C contains a calculation of the energy shift at the strong-coupling fixed point to lowest order in perturbation theory, for the completely antisymmetric impurity. Since the ground state is a singlet, there is no splitting of levels. Nevertheless, the behavior of the energy with the filling, n_d, on the neighboring site shares many common features with the problem that we have studied. Finally, we include the details of the calculation of the matrix elements needed in the second-order perturbation theory calculation in Appendix D. We also include several sets of SU(N) Clebsch-Gordan coefficients that we had to evaluate explicitely for arbitrary $2S$, q, and n_d.

II. THE MODEL AND ITS STRONG-COUPLING LIMIT

Here we present the model that we study as well as its ground state and elementary excitations in the strong-coupling ($J=\infty$) limit. The results summarized in this section were already obtained in Refs. 26 and 27. However, technical details such as the explicit form of the eigenstates included in Appendix B, are original.

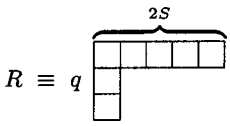

FIG. 1. Young tableau description of an impurity with mixed symmetry, $[2S,1^{q-1}]$, realized by a combination of fermions and bosons.

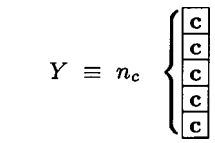

FIG. 2. Young tableau description of n_c conduction electrons, *localized* at the impurity site.

A. SU(N) single-impurity Kondo model

We consider a generalized, single-impurity, Kondo model with one channel of conduction electrons and a spin symmetry group extended from SU(2) to SU(N). An impurity spin $\mathbf{S}$ is placed at the origin (site 0). In this paper we will deal with impurities that can be realized by a combination of bosonic and fermionic operators, and are thus described by a L-shaped representation in the language of Young tableaux,[35–37] as illustrated in Fig. 1 (for details, see Appendix B).

If $2S$ and q are the numbers of boxes along the first row and the first column, respectively, the representation is denoted by $[2S,1^{q-1}]$. Its degeneracy[38] is reported in Table I. The conduction electrons transform under the fundamental representation of SU(N) and can be represented by Young tableaux made out of single boxes. The dimension of the fundamental representation is N, which just means that each electron can be in one of N states of spin.

The Hamiltonian describing the model is written as

$$H=\sum_{\mathbf{k},\alpha}\varepsilon_{\mathbf{k}}c^{\dagger}_{\mathbf{k},\alpha}c_{\mathbf{k},\alpha}+J\sum_{A}\mathbf{S}^{A}\sum_{\alpha,\beta}c^{\dagger}_{\alpha}(0)\boldsymbol{\tau}^{A}_{\alpha\beta}c_{\beta}(0), \quad (2)$$

where $c^{\dagger}_{\mathbf{k},\alpha}$ is the creation operator of a conduction electron with momentum $\mathbf{k}$, SU(N) spin index $\alpha=a,b,\ldots,r_N$, $c^{\dagger}_{\alpha}(0)=1/\sqrt{N_S}\Sigma_{\mathbf{k}}c^{\dagger}_{\mathbf{k},\alpha}$ is the creation operator of a conduction electron at the origin, N_S is the number of sites, and $\boldsymbol{\tau}^{A}_{\alpha\beta}$ ($A=1,\ldots,N^2-1$) are the generators of the SU(N) group in the fundamental representation, with $\mathrm{Tr}[\boldsymbol{\tau}^{A}\boldsymbol{\tau}^{B}]=\delta_{AB}/2$. In the SU(2) case, $\boldsymbol{\tau}^{A}=\boldsymbol{\sigma}^{A}/2$, where $\{\boldsymbol{\sigma}^{A}\}$ are the Pauli matrices. The conduction electrons interact with the impurity spin $\mathbf{S}^{A}$ ($A=1,\ldots,N^2-1$), placed at the origin, via Kondo coupling, $J>0$. When the impurity is in the fundamental representation, we recover the Coqblin-Schrieffer model[30,39] describing conduction electrons in interaction with an impurity spin of angular momentum j, ($N=2j+1$), resulting of the combined spin and orbit exchange scattering. In our notation, $a=j,\ b=j-1,\ldots,r_N=-j$.

B. Strong-coupling fixed point

In the strong-coupling limit, the Hamiltonian reduces to the local Kondo interaction term at site 0,

$$H=J\sum_{A}\mathbf{S}^{A}\sum_{\alpha,\beta}c^{\dagger}_{\alpha}(0)\boldsymbol{\tau}^{A}_{\alpha\beta}c_{\beta}(0). \quad (3)$$

The ground state, $|\mathrm{GS}\rangle$, is formed by binding the right amount of conduction electrons to the impurity in order to minimize the Kondo energy. Let us denote by Y (Fig. 2) the representation of the n_c conduction electrons coupled to the impurity, R that of the free impurity (Fig. 1), and R_{SC} the representation of one of the strong-coupling states resulting of the direct product $R\otimes Y$ (cf. Fig. 3) (see Appendix B for details).

When $N=2$, the Kondo energy can be written in terms of conserved quantities

$$J\vec{\mathbf{S}}\cdot\sum_{\alpha,\beta}c^{\dagger}_{\alpha}(0)\vec{\boldsymbol{\tau}}_{\alpha\beta}c_{\beta}(0)\ |\mathrm{GS}\rangle$$
$$=\frac{J}{2}[S^{SC}(S^{SC}+1)-S^{R}(S^{R}+1)-S^{Y}(S^{Y}+1)]|\mathrm{GS}\rangle,$$

where $S(S+1)$ is the eigenvalue of the Casimir operator $\hat{S}^2$ for $N=2$. The generalization to SU(N) is given by

$$J\sum_{A}\mathbf{s}^{A}\sum_{\alpha,\beta}c^{\dagger}_{\alpha}(0)\boldsymbol{\tau}^{A}_{\alpha\beta}c_{\beta}(0)|\mathrm{GS}\rangle$$
$$=\frac{J}{2}[\hat{\mathcal{C}}_2(R_{SC})-\hat{\mathcal{C}}_2(R)-\hat{\mathcal{C}}_2(Y)]|\mathrm{GS}\rangle, \quad (4)$$

TABLE I. Dimension d and eigenvalues of the Casimir operator $\mathcal{C}_2$ for the symmetric, antisymmetric, L-shaped, and fundamental representations studied in this paper. In the L-shaped case, $Q=(2S+q-1)$ is the total number of boxes in the Young tableau, and $Y'=(q-2S)$ measures the row-column asymmetry.

	Symmetric $[2S]$	Antisymmetric $[1^q]$	L shaped $[2S,1^{q-1}]$	Fundamental $[1]$
d	C^{2S}_{N+2S-1}	C^{q}_{N}	$\left(\frac{2S}{2S+q-1}\right)C^{2S}_{N+2S-1}C^{q-1}_{N-1}$	N
$\mathcal{C}_2$	$\frac{1}{2N}[2S(2S+N)(N-1)]$	$\frac{1}{2N}[q(N-q)(N+1)]$	$\frac{Q}{2}(N-Y'-Q/N)$	$\frac{1}{2N}(N^2-1)$

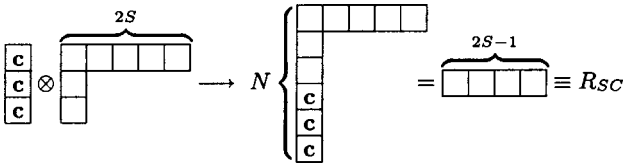

FIG. 3. Young tableau description of the formation of the strong coupling ground state. We denote the presence of conduction electrons at site 0 by **c**. Notice that the first column in the Young tableau for R_{SC} is a singlet and can be removed.

where $\mathcal{C}_2(\hat{R})$ is the quadratic Casimir operator of the representation $\hat{R}$, which commutes with all the generators of the group. For a representation given by a Young tableau with m_j boxes in the jth row until the row $j=h<N$, the eigenvalue $\mathcal{C}_2(\{m_j\})$ of the quadratic Casimir operator is

$$\mathcal{C}_2(\{m_j\})=\frac{1}{2}\left[\frac{Q(N^2-Q)}{N}+\sum_{j=1}^{h} m_j(m_j+1-2j)\right],$$

where $Q=\Sigma_{j=1}^{h} m_j$ is the total number of boxes.[40] Table I summarizes the expressions of the Casimir eigenvalues for the impurities described in this work and for the conduction electrons, as well as the dimension of their spin representations.

Minimization of the energy, Eq. (4), leads to a ground state with $n_c=(N-q)$ conduction electrons coupled to the L-shaped Kondo impurity ensuring partial screening. The resulting composite at site 0, with energy E_0, is made out of the impurity dressed by the conduction electrons in order to form a singlet along the first column. The associated Young tableau in the strong-coupling regime is given in Fig. 3. Note that the first column of length N can be removed without changing the representation since it is a singlet. When the strong-coupling fixed point is stable, this corresponds to a one-stage Kondo effect in which the impurity is screened by the conduction electrons to form a bosonic $(S-1/2)$ impurity.

C. Ground state

Let us now write the expression of the fundamental state associated with this strong-coupling fixed point. The ground state is degenerate. The states in the multiplet transform as a completely symmetric representation of SU(N), described by a Young tableau with $(2S-1)$ boxes, denoted by $[2S-1]$ (Fig. 3). We choose a realization of the impurity in terms of $2S$ bosonic operators and $(q-1)$ fermionic operators, which happens to be more convenient. We could have constructed impurity states with the same SU(N) symmetry using $(2S-1)$ bosons and q fermions (see Appendix B). We would like to emphasize that all the results that we establish in this paper are independent of the operator representation which we choose to work with. The highest weight state is then written as

$$|\mathrm{GS}\rangle_{\{a\}aa}^{[2S-1]}=\frac{1}{\sqrt{(2S-1)!}}(b_a^\dagger)^{2S-1}|\Delta\rangle \qquad (5)$$

with

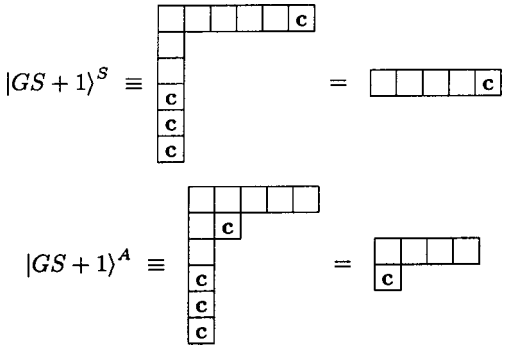

FIG. 4. Excited states $|\mathrm{GS}+1\rangle^S$ and $|\mathrm{GS}+1\rangle^A$ with an additional conduction electron $n_c=(N-q+1)$, respectively, in the symmetric and antisymmetric configurations.

$$|\Delta\rangle\equiv\frac{1}{\gamma}\mathcal{A}\left[b_{i_1}^\dagger\left(\prod_{\alpha=i_2}^{i_q} f_\alpha^\dagger\right)\left(\prod_{\beta=i_{q+1}}^{i_N} c_\beta^\dagger\right)\right]|0\rangle, \qquad (6)$$

$$\gamma\equiv\sqrt{(2S+N-1)C_{N-1}^{q-1}}.$$

Here, $|\Delta\rangle$ transforms itself as a SU(N) singlet and it will be annihilated by any of the raising and lowering operators, $T^\pm|\Delta\rangle=U^\pm|\Delta\rangle=\cdots=0$. This "state" would describe the strong-coupling ground state for a purely fermionic impurity.

D. Excited states

There are two types of excited states in the strong-coupling regime. Either the degenerate ground state acquires an additional conduction electron at the impurity site $|\mathrm{GS}+1\rangle$, or it loses one conduction electron, $|\mathrm{GS}-1\rangle$. In the former case $|\mathrm{GS}+1\rangle$ the spin of the additional conduction electron can be either symmetrically or antisymmetrically correlated with the spin of the impurity as schematized in Fig. 4.

In the limiting case of SU(2) spin, these two configurations correspond to a spin of the conduction electron that is either parallel or antiparallel to the impurity spin. In the general SU(N) case, we will keep on speaking of symmetric and antisymmetric configurations, respectively.

States with one less electron will be denoted by $|\mathrm{GS}-1\rangle$ and are represented by the Young tableau in Fig. 5. Let us denote by $\Delta E_1^S=E_1^S-E_0$, $\Delta E_1^A=E_1^A-E_0$, and $\Delta E_2=E_2-E_0$ the energy differences, with respect to the ground-state energy, associated with these three excited states $|\mathrm{GS}+1\rangle^S$, $|\mathrm{GS}+1\rangle^A$, and $|\mathrm{GS}-1\rangle$. Using the same Casimirology method as presented at the beginning of this section for the determination of the ground-state energy, we have summarized our results in Table II, respectively, for arbitrary N and in the large-N limit with $(2S+q-1)/N$ finite. One can

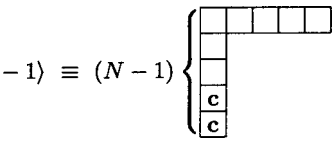

FIG. 5. Excited state $|\mathrm{GS}-1\rangle$ with one less conduction electron $n_c=(N-q-1)$.

TABLE II. Strong-coupling excitation energies, ΔE_1^S, ΔE_1^A, and ΔE_2, in the case of an L-shaped impurity, measured with respect to the ground state, of the states with one more conduction electron on site 0, coupled symmetrically and antisymmetrically, respectively, to the dressed impurity on site 0, and of the state with one less electron.

	ΔE_1^S	ΔE_1^A	ΔE_2
Arbitrary N	$\frac{J}{2}(2S+N-q-Q/N)$	$\frac{J}{2}(N-q-Q/N)$	$\frac{J}{2}(q+Q/N)$
Large N limit (Q/N finite)	$\frac{J}{2}(N-q+2S)$	$\frac{J}{2}(N-q)$	$\frac{J}{2}q$

check that the results in Table II coincide with Eqs. (25) and (26) of Ref. 27, within a $N/2$ factor stemming from a different definition of the Kondo coupling J [cf. Eq. (1)of Ref. 27] and of the Casimir [cf. Eq. (17) of Ref. 27], and a change in the notations $n_f^*=q$ and $n_b=2S$.

Notice that the excitation energies ΔE_1^A and ΔE_2, in the large N limit, are independent of S, and related by the *particle-hole* transformation $q\rightarrow N-q$, characteristic of the problem with a purely antisymmetric impurity, $2S=1$ (see Appendix C).

III. STABILITY OF THE STRONG-COUPLING FIXED POINT

We have identified the strong-coupling fixed point in the preceding section. For $J\rightarrow\infty$, the lowest energy state corresponds to $n_c=(N-q)$ electrons partially screening the impurity at the origin, and isolated from the rest of the bulk which may be described by a chain of electrons, for convenience.

In order to better understand the low-energy physics of the system, we can perform a strong-coupling analysis considering a finite Kondo coupling and allowing virtual hopping from and to the impurity site. These processes generate interactions between the composite at site 0 and the conduction electrons on neighboring sites, which can be treated as perturbations of the strong-coupling fixed point. Applying an analysis similar to that of Nozières and Blandin[31] to the nature of the excitations, we can argue whether or not the strong-coupling fixed point remains stable once virtual hopping is allowed.

We consider a system with an additional site next to the dressed impurity, filled with n_d electrons. The ground state consists of two multiplets, with different symmetry properties. Once the hopping is turned on, the degeneracy is lifted, and each multiplet acquires a different energy shift denoted by ΔE^S and ΔE^A, respectively (see Fig. 6). We can reproduce this spectrum by considering an effective coupling between the spin of the dressed spin at site 0, and the spin of the n_d electrons on site 1. If E^S lies (above) below E^A, the effective coupling is (antiferromagnetic) ferromagnetic.

Thus, if the coupling between the effective spin at the impurity site and that of the electrons on site 1 is ferromagnetic we know, from the scaling analysis at weak coupling, that the perturbation is irrelevant, and the low-energy physics is described by the strong-coupling fixed point. That is, an underscreened, completely symmetric, effective impurity weakly coupled to a gas of free electrons with a phase shift indicating that there are already $(N-q)$ electrons screening the original impurity. In the completely antisymmetric case $(2S=1)$, the phase shift corresponds to the unitary limit, $\delta=\pi/2$, for SU(2), and is a function[41] of q/N for SU(N), reaching the unitary limit for $q=N/2$.

If, on the contrary, the effective coupling is antiferromagnetic, the perturbation is relevant, this strong-coupling fixed point is unstable and it does not describe the low-energy physics of the model.

In this section we explicitely calculate the effects of hopping on the strong-coupling fixed point to the lowest order in perturbation theory, that is, second order in t. We will consider the case with an arbitrary number n_d of conduction electrons in site 1 generalizing the case $n_d=1$ considered in Ref. 27. This will allow us to understand the origin of the instability of the strong-coupling fixed point.

Before switching on the hopping term, let us consider *ground states* of the form $|\mathrm{GS},n_d\rangle=\Sigma|\mathrm{GS}\rangle_0|n_d\rangle_1$, with n_d

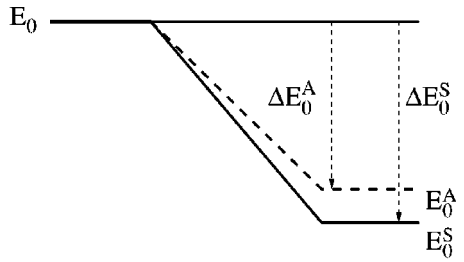

(a) ferromagnetic effective coupling case

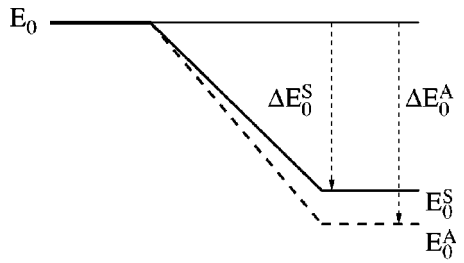

(b) antiferromagnetic effective coupling case

FIG. 6. Second-order perturbation theory energy shift of the strong-coupling ground state in the cases of a ferromagnetic (a) and antiferromagnetic (b) effective coupling.

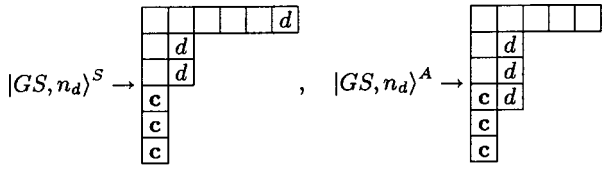

FIG. 7. Strong-coupling ground states in the presence of n_d conduction electrons on site 1 coupled either symmetrically or antisymmetrically to the dressed impurity on site 0.

electrons on site 1. According to the SU(N) symmetry there are two possible configurations, depending on whether the n_d electrons are coupled symmetrically or antisymmetrically to the composite on site 0. This corresponds to the Clebsch-Gordan series $[2S-1]\otimes[n_d]\rightarrow[2S,1^{n_d-1}]\oplus[2S-1,1^{n_d}]$. We denote the states by $|\mathrm{GS},n_d\rangle^S$, and $|\mathrm{GS},n_d\rangle^A$, respectively (Fig. 7).

The SU(N) symmetry is preserved by the hopping. That means that the perturbation will shift the energies of $|\mathrm{GS},n_d\rangle^S$ and $|\mathrm{GS},n_d\rangle^A$ separately, without mixing the states. We will thus denote the shifts by ΔE_0^S and ΔE_0^A, respectively.

The hopping term is of the form

$$H_h=H_1+H_2=t\sum_\alpha c_\alpha^\dagger d_\alpha+t\sum_\alpha d_\alpha^\dagger c_\alpha, \quad (H_1)^\dagger=H_2,$$

where $d_\alpha^\dagger$ creates an electron on site 1. We can distinguish two types of processes, corresponding to different intermediate states.[27] The first type, which we denote process 1, corresponds to an electron hopping from site 1 into site 0 first, probing excited states $|\mathrm{GS}+1\rangle^{S,A}$, and then hopping back to site 1. The indices S,A correspond to the two possible intermediate states depending on whether the conduction electron that hops to site 0 is symmetrically or antisymmetrically correlated with the dressed impurity as we will see in detail below. The contribution of the process 1 to the energy shift is the following:

$$t^2\sum_{\alpha,\beta}\sum_i \frac{\langle \mathrm{GS},n_d|d_\beta^\dagger c_\beta|\mathrm{GS}+1,n_d-1\rangle^{ii}\langle \mathrm{GS}+1,n_d-1|c_\alpha^\dagger d_\alpha|\mathrm{GS},n_d\rangle}{(E_0-E_1^i)},$$

with $i=S,A$ (see Appendix B).

In process 2, the electron hops from site 0 to site 1 first and then back to site 0, probing $|\mathrm{GS}-1\rangle$, leading to a contribution to the energy shift of the form

$$t^2\sum_{\alpha,\beta}\frac{\langle \mathrm{GS},n_d|c_\beta^\dagger d_\beta|\mathrm{GS}-1,n_d+1\rangle\langle \mathrm{GS}-1,n_d+1|d_\alpha^\dagger c_\alpha|\mathrm{GS},n_d\rangle}{(E_0-E_2)}.$$

Hence, the energy shifts for the symmetric and antisymmetric configurations are, respectively,

$$\Delta E_0^S=\frac{M_1^S}{E_0-E_1^S}+\frac{\overline{M_1^S}}{E_0-E_1^A}+\frac{M_2^S}{E_0-E_2}, \tag{7}$$

$$\Delta E_0^A=\frac{M_1^A}{E_0-E_1^A}+\frac{M_2^A}{E_0-E_2}, \tag{8}$$

where the expressions in the denominators, $(E_0-E_1^S)=-\Delta E_1^S$, $(E_0-E_1^A)=-\Delta E_1^A$, and $(E_0-E_2)=-\Delta E_2$ measuring the energy of the excited states compared to the energy of the ground state are given in Table II. The matrix elements M will be introduced below as we will study the contribution of each process. The energy difference between the two states,

$$\Delta E_0^S-\Delta E_0^A=\frac{M_1^S}{E_0-E_1^S}+\frac{\overline{M_1^S}-M_1^A}{E_0-E_1^A}+\frac{M_2^S-M_2^A}{E_0-E_2}, \tag{9}$$

determines the sign of the effective interaction and the stability of the strong-coupling fixed point. If we compare Eq. (9) to the $n_d=1$ result in Ref. 27, we see that there is an additional contribution $\overline{M_1^S}$, present for $n_d>1$.

A. Process 1: Symmetric configuration

We consider first the case where the n_d electrons in the site 1 are coupled to the site-0 state in the most symmetric configuration. In the shorthand notation that we use for the Young tableaux, it corresponds to the state $[2S-1]\otimes[1^{n_d}]\rightarrow[2S,1^{n_d-1}]$. Here, as opposed[27] to the case $n_d=1$, the Hamiltonian transforms the ground state

$$|\mathrm{GS},n_d\rangle^S=(d_a^\dagger d_b^\dagger\cdots d_u^\dagger)|\mathrm{GS}\rangle, \tag{10}$$

into a linear combination of two excited states: $|\mathrm{GS}+1,n_d-1\rangle^S$, with energy E_S, and $|\overline{\mathrm{GS}+1,n_d-1}\rangle^S$, with energy E_A depending on whether the additional conduction electron in site 0 is coupled symmetrically or antisymmetrically to the dressed impurity. The state obtained by acting with $c_\sigma^\dagger d_\sigma$ on the ground state defined by Eq. (10) has to be computed explicitely, and the result written as a linear combination of the excited states, Fig. 8. The latter are obtained by coupling the site-0 states with (n_d-1) conduction electrons on site 1.

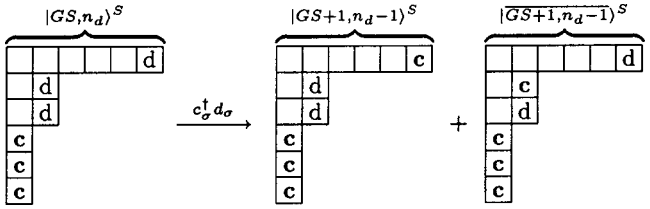

FIG. 8. When n_d conduction electrons are coupled symmetrically to the dressed impurity at the origin, the term $c_\sigma^\dagger d_\sigma$, acting on the ground state, generates a linear combination of two excited states with an additional conduction electron at the origin.

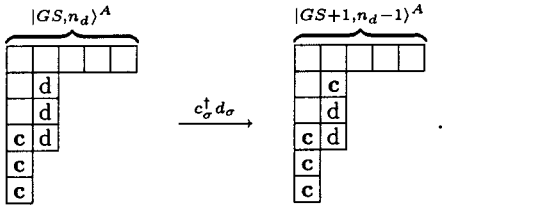

FIG. 9. When n_d conduction electrons are coupled antisymmetrically to the dressed impurity at the origin, the term $c_\sigma^\dagger d_\sigma$, acting on the ground state, generates state proportional to a given excited state, with additional conduction electron at the origin.

The explicit expressions for these states are given in Appendix D, and they lead to the result

$$\left(\sum_\sigma c_\sigma^\dagger d_\sigma\right)|\mathrm{GS},n_d\rangle^S = \Omega\sqrt{\frac{2S+n_d-1}{2S}}|\mathrm{GS}+1,n_d-1\rangle^S + \Lambda\sqrt{n_d-1}\sqrt{\frac{2S-1}{2S}}|\overline{\mathrm{GS}+1,n_d-1}\rangle^S, \tag{11}$$

where the normalization coefficients,[27] $\Omega=\sqrt{(2S+q-1)/(2S+N-1)}$ and $\Lambda=\sqrt{(q-1)/(N-1)}$ are independent of n_d, as we are considering hopping of a single electron. From here, we obtain the following matrix elements:

$$M_1^S=|^S\langle \mathrm{GS}+1,n_d-1|H_1|\mathrm{GS},n_d\rangle^S|^2 = t^2\left(\frac{2S+n_d-1}{2S}\right)\left(\frac{2S+q-1}{2S+N-1}\right), \tag{12}$$

$$\overline{M_1^S}=|^S\langle\overline{\mathrm{GS}+1,n_d-1}|H_1|\mathrm{GS},n_d\rangle^S|^2 = t^2(n_d-1)\left(\frac{2S-1}{2S}\right)\left(\frac{q-1}{N-1}\right). \tag{13}$$

We see right away that $\overline{M_1^S}$ is proportional to (n_d-1), and vanishes for $n_d=1$, whereas M_1^S depends noticeably on n_d only for $2S\ll n_d<N$.

B. Process 1: Antisymmetric configuration

Next, we consider the case where the electrons on site 1 are coupled to the effective spin on site 0 according to $[2S-1]\otimes[1^{n_d}]\to[2S-1,1^{n_d}]$. In the preceding section it was easy to write the strong-coupling ground state by just putting together the effective spin and the n_d electrons in the highest weight state possible, to obtain Eq. (10). Here we have to work out the necessary SU(N) Clebsch-Gordan coefficients. We present some of these coefficients in Table VII of Appendix D. The explicit form of the ground state is

$$|\mathrm{GS},n_d\rangle^A_{abc\ldots v}=\frac{1}{\sqrt{2S+n_d-1}}\left[\sqrt{2S-1}\left(\prod_{i=2}^{n_d+1} d_{y_i}^\dagger\right)|\mathrm{GS}\rangle_{aa} + \sum_{j=2}^{n_d+1}(-1)^{j-1}\left(\prod_{i=1,i\neq j}^{n_d+1} d_{y_i}^\dagger\right)|\mathrm{GS}\rangle_{ay_j}\right], \tag{14}$$

in the notation $y_1=a$. As in the $n_d=1$ case, the hopping term transforms the state defined by Eq. (14) into a state proportional to a given strong-coupling excited state (Fig. 9). In order to obtain the corresponding matrix element, we have computed explicitly

$$\left(\sum_\sigma c_\sigma^\dagger d_\sigma\right)|\mathrm{GS},n_d\rangle^A \propto|\mathrm{GS}+1,n_d-1\rangle^A,$$

and then we have normalized the resulting state. The details can be found in Appendix D. We have

$$\left(\sum_\sigma c_\sigma^\dagger d_\sigma\right)|\mathrm{GS},n_d\rangle^A=\Lambda\sqrt{n_d}|\mathrm{GS}+1,n_d-1\rangle^A,$$

and the matrix element

$$M_1^A=|^A\langle \mathrm{GS}+1,n_d-1|H_1|\mathrm{GS},n_d\rangle^A|^2=t^2n_d\left(\frac{q-1}{N-1}\right). \tag{15}$$

Notice the dependence on n_d, and the fact that the matrix element does not depend on $2S$. Combining together $\overline{M_1^S}$ and M_1^A as it appears in Eq. (9), we have

$$\overline{M_1^S}-M_1^A=-t^2\left(\frac{2S+n_d-1}{2S}\right)\left(\frac{q-1}{N-1}\right). \tag{16}$$

This is a term with the same n_d dependence as M_1^S but with the opposite sign.

C. Process 2: The trick

Both in the symmetric and antisymmetric configurations in process 2 there is a one-to-one correspondence between the state obtained by the action of H_2, and the excited state with the same symmetry[27] (Fig. 10). The evaluation of the remaining matrix elements, M_2^S and M_2^A, associated with process 2 is simplified by using the following trick connecting the matrix elements of processes 1 and 2, respectively. On the one hand, we have in the process 1,

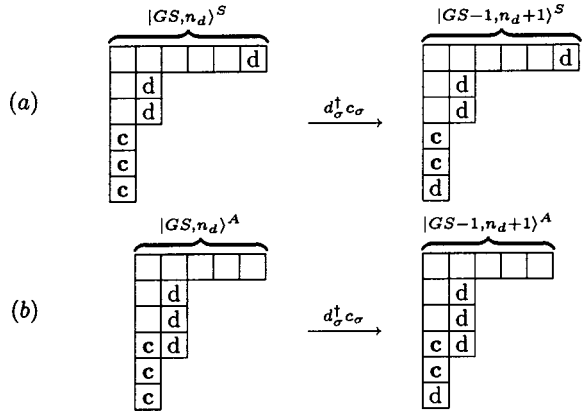

FIG. 10. The term $d_\sigma^\dagger c_\sigma$, acting on the ground state with n_d electrons on site 1, coupled symmetrically (a) or antisymmetrically (b) to the impurity. The result is a state proportional to an excited state with one less electron at the impurity site, coupled to (n_d+1) electrons symmetrically (a) or antisymmetrically (b).

$$M_1^S+\overline{M_1^S}=t^2\sum_{\sigma\sigma'}{}^S\ \langle \mathrm{GS},n_d|d_{\sigma'}^\dagger c_{\sigma'}c_\sigma^\dagger d_\sigma|\mathrm{GS},n_d\rangle^S$$

$$=t^2\sum_{\sigma\sigma'}{}^S\ \langle d_{\sigma'}^\dagger(\delta_{\sigma\sigma'}-c_\sigma^\dagger c_{\sigma'})d_\sigma\rangle^S$$

$$=t^2\sum_{\sigma}{}^S\ \langle d_\sigma^\dagger d_\sigma\rangle^S-\delta M^S,$$

where $\delta M^S=t^2\Sigma_{\sigma\sigma'}{}^S\langle c_\sigma^\dagger d_{\sigma'}^\dagger d_\sigma c_{\sigma'}\rangle^S$ and the expectation value ${}^S\langle\rangle^S$ should be considered over the ground state, $|\mathrm{GS},n_d\rangle^S$. On the other hand, the following property holds for the matrix elements of process 2

$$M_2^S=t^2\sum_{\sigma\sigma'}{}^S\ \langle \mathrm{GS},n_d|c_{\sigma'}^\dagger d_{\sigma'}d_\sigma^\dagger c_\sigma|\mathrm{GS},n_d\rangle^S$$

$$=t^2\sum{}^S\sigma\sigma'\langle c_{\sigma'}^\dagger(\delta_{\sigma\sigma'}-d_\sigma^\dagger d_{\sigma'})c_\sigma\rangle^S$$

$$=t^2\sum_{\sigma}{}^S\ \langle c_\sigma^\dagger c_\sigma\rangle^S-\delta M^S,$$

where in the last line, we have exchanged the dummy variables σ and σ'. The same relation exists for the antisymmetric configuration (with expectation values taken on $|\mathrm{GS},n_d\rangle^A$)

$$M_1^A=t^2\sum_{\sigma}{}^A\ \langle d_\sigma^\dagger d_\sigma\rangle^A-\delta M^A,$$

$$M_2^A=t^2\sum_{\sigma}{}^A\ \langle c_\sigma^\dagger c_\sigma\rangle^A-\delta M^A.$$

Thus, using the trick, we obtain

$$M_2^S=t^2(n_c-n_d)+(M_1^S+\overline{M_1^S})$$

$$=t^2(N-n_d)\left(\frac{N-q}{N-1}\right)\left(\frac{2S+N-2}{2S+N-1}\right), \tag{17}$$

$$M_2^A=t^2(n_c-n_d)+M_1^A=t^2[N-(n_d+1)]\left(\frac{N-q}{N-1}\right), \tag{18}$$

$$M_2^S-M_2^A=M_1^S+\overline{M_1^S}-M_1^A=t^2\left(\frac{2S+n_d-1}{2S+N-1}\right)\left(\frac{N-q}{N-1}\right). \tag{19}$$

IV. DISCUSSION

Having computed the different matrix elements in the preceding section, we are now in the position of deriving the expressions of the energy shifts ΔE_0^S and ΔE_0^A of the symmetric and antisymmetric configurations, respectively, within the second-order perturbation theory in the hopping term. We propose to transcribe the results in terms of an effective Hamiltonian describing the charge and spin interactions between the dressed impurity at site 0, and the conduction electrons in amount n_d at site 1. We will then discuss the implications of the derived effective Hamiltonian on the behavior of the system.

(i) The sign of the effective coupling—ferromagnetic versus antiferromagnetic—controlling the stability of the strong-coupling fixed point, determines the onset of two different regimes. When $q<N/2$, the effective coupling is found to be ferromagnetic, the perturbation is proved to be irrelevant by use of scaling arguments [cf. Eq. (1)], and the strong-coupling fixed point is stable. When $q>N/2$, on the contrary, the effective coupling is found to be antiferromagnetic, the perturbation becomes relevant, and the strong-coupling fixed point is unstable.

(ii) There is an effective charge interaction at site 1, induced by the virtual hopping of electrons between the impurity site and its nearest-neighbor site. The change in the nature of this interaction—from repulsive to attractive—is found to happen at the same place where the strong-coupling fixed point becomes unstable. On the one hand, in the regime when the strong-coupling fixed point is stable $q<N/2$, the interaction is repulsive. On the other hand, in the regime $q>N/2$, the interaction is attractive. However, we emphasize the point that this attraction is never realized as such since the strong-coupling fixed point is then unstable.

Even though the charge interaction remains a weak perturbation of the full system, its study allows us to better understand the physical properties of the model and the onset of instability of the strong-coupling fixed point at a particular value of q. Indeed, this charge interaction is already present in the case of an antisymmetric impurity, as we will show below. There, the low-energy physics is controlled by the strong-coupling fixed point for all values of q. Nevertheless, there is a change in the sign of the effective charge interaction at $q=N/2$, a consequence of the $q\rightarrow N-q$ symmetry in the antisymmetric case. The fact that the coupling U_{eff} is the same (in the large N limit) for the general L-shaped impurity as for the completely antisymmetric case, indicates that the properties observed in the former case are linked to the $q\rightarrow N-q$ transformation of the fermionic component of the impurity.

A. Energy shifts ΔE_0^S and ΔE_0^A

Incorporating the expressions of the matrix elements, Eqs. (12), (16), and (19), and those of the excitation energies (Table II) into Eqs. (8) and (9), one finds

$$\Delta E_0^A = -\left(\frac{2t^2}{J}\right)\left[\left(\frac{n_d}{N-1}\right)\left(\frac{q-1}{N-q-Q/N}\right) + \left(1-\frac{n_d}{N-1}\right)\left(\frac{N-q}{q+Q/N}\right)\right], \tag{20}$$

$$\Delta E_0^S - \Delta E_0^A = -(2S+n_d-1)\left(\frac{2t^2}{J}\right) \times\left\{\frac{2S+q-1}{2S(2S+N-1)[2S+N-q-(2S+q-1)/N]} + \frac{N-q}{(N-1)(2S+N-1)[q+(2S+q-1)/N]} - \frac{q-1}{2S(N-1)[N-q-(2S+q-1)/N]}\right\}. \tag{21}$$

The dependence of $(\Delta E_0^S - \Delta E_0^A)$ on $(2S+n_d-1)$ is linear and appears factored out. As $2S$ increases, the energy difference $(\Delta E_0^S - \Delta E_0^A)$ becomes smaller. Moreover, the effect of n_d on $(\Delta E_0^S - \Delta E_0^A)$ is weak as long as $n_d \ll 2S$.

Until now, we have presented results for arbitrary N. In the rest of the paper, we will frequently consider the large-N limit taking $2S/N$ and q/N finite. To leading order in $1/N$, we can write

$$\Delta E_0^A = -\frac{2t^2}{J}\left[\left(\frac{N-q}{q}\right) - \left(\frac{n_d}{N}\right)\left(\frac{N(N-2q)}{q(N-q)}\right)\right], \tag{22}$$

$$\Delta E_0^S - \Delta E_0^A = -\frac{2t^2}{JN}\left(\frac{2S+n_d-1}{2S+N-q}\right)\left(\frac{N(N-2q)}{q(N-q)}\right). \tag{23}$$

The energy difference $(\Delta E_0^S - \Delta E_0^A)$ is $O(1/N)$, and both energy levels, ΔE_0^S and ΔE_0^A, have the same leading term in $O(1)$ which is almost independent of $2S$. The only dependence in $2S$ appears in the difference $(\Delta E_0^S - \Delta E_0^A)$.

B. Effective Hamiltonian

The energy shifts ΔE_0^S and ΔE_0^A can be reproduced from the following effective Hamiltonian, to within an additive constant term C to be defined later on,

$$H_{eff} = U_{eff}\, n_d + J_{eff}\mathbf{S}_0^{[2S-1]}\cdot\mathbf{S}_1^{[1^{n_d}]},$$

where U_{eff} and J_{eff} are the effective charge and spin interactions, respectively, between the dressed impurity at site 0 in the strong-coupling limit and the conduction electrons at site 1. In the notations which are used, $\mathbf{S}_0^{[2S-1]}$ and $\mathbf{S}_1^{[1^{n_d}]}$ represent the corresponding spin operators in the representations $[2S-1]$ and $[1^{n_d}]$, respectively. The spectrum consists of two multiplets, according to the Clebsh-Gordan series $[2S-1]\otimes[1^{n_d}] \to [2S,1^{n_d-1}]^S \oplus [2S-1,1^{n_d}]^A$, in which the superindices S and A indicate the symmetric and antisymmetric states, respectively. The energies shifts induced by H_{eff} can be calculated as before with the aid of Casimir operators, Eq. (4), and we get

$$\begin{aligned}\Delta E^S_{[2S,1^{n_d-1}]} - \Delta E^A_{[2S-1,1^{n_d}]} &= \frac{J_{eff}}{2}\{\mathcal{C}_2([2S,1^{n_d-1}]) - \mathcal{C}_2([2S-1,1^{n_d}])\} \\ &= -\frac{J_{eff}}{4}(2S+n_d-1)[Y'_{[2S,1^{n_d-1}]} - Y'_{[2S-1,1^{n_d}]}] \\ &= \frac{J_{eff}}{2}(2S+n_d-1),\end{aligned}$$

where we have used the results of Table I. Since both states have Young tableaux with the same number of boxes, $Q_{eff} = 2S+n_d-1$, the energy difference depends only on the second constraint (B7), $\hat{\mathcal{Y}}_{eff} = Q_{eff}Y'$ (see Appendix B). As a consequence, the dependence on $(2S+n_d-1)$ is factored out exactly as in Eq. (21) and we get by identification

$$J_{eff} = -\left(\frac{4t^2}{J}\right) \times\left\{\frac{2S+q-1}{2S(2S+N-1)[2S+N-q-(2S+q-1)/N]} + \frac{N-q}{(N-1)[2S+N-1)(q+(2S+q-1)/N]} - \frac{q-1}{2S(N-1)[N-q-(2S+q-1)/N]}\right\}, \tag{24}$$

$$U_{eff} = \frac{2t^2}{J}\,\frac{1}{N-1}\left(\frac{N-q}{q+Q/N} - \frac{q-1}{N-q-Q/N}\right) \tag{25}$$

with the additive constant term C equal to $(-2t^2/J)(N-q)/(q+Q/N)$.

In the large-N limit with $2S/N$ and q/N finite, we have

$$J_{eff} = -\frac{4t^2}{J}\,\frac{(N-2q)}{q(N-q)}\,\frac{1}{(2S+N-q)}, \tag{26}$$

$$U_{eff} = \frac{2t^2}{J}\,\frac{(N-2q)}{q(N-q)} \tag{27}$$

with C equal to $(-2t^2/J)(N-q)/q$. Note that J_{eff} is $O(1/N^2)$ and depends of $2S$, while U_{eff} is $O(1/N)$ and independent of $2S$. Furthermore, U_{eff} is repulsive when J_{eff} is ferromagnetic, and attractive when J_{eff} is antiferromagnetic.

C. Sign of the effective coupling and stability of the strong-coupling fixed point

In Fig. 11 we plot J_{eff} in the large-N limit as a function of q/N, for different values of $2S$. The effective coupling J_{eff}

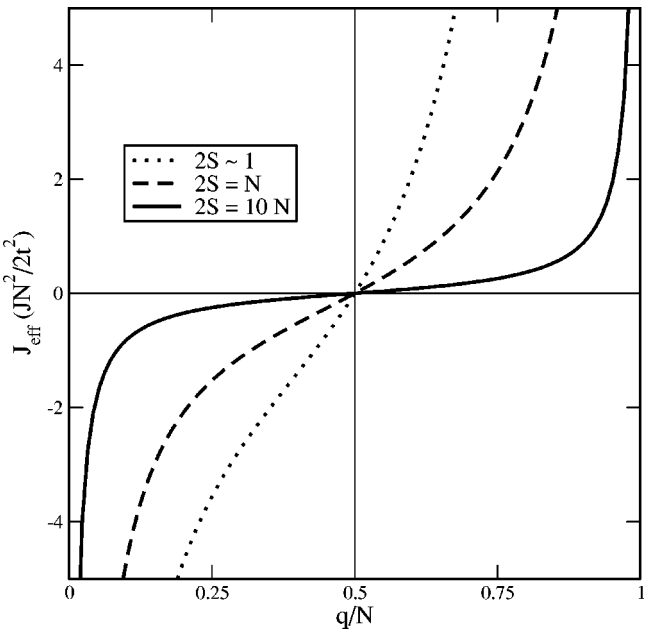

FIG. 11. Effective coupling J_{eff} as a function of q/N, for different values of $2S$, in the large-N limit.

changes of sign at $q=N/2$ as can be seen by inspection of the numerator of the right-hand side of Eq. (26). Notice that the value of J_{eff} is independent of the number of conduction electrons n_d on site 1 and coincides with the result obtained in Ref. 27 for the case $n_d=1$. This is due to the cancellation of the $(2S+n_d-1)$ factor in $(\Delta E_0^S-\Delta E_0^A)$ that we have mentioned above.

The effective coupling remains ferromagnetic as long as $q<N/2$ corresponding to the situation $E_0^S<E_0^A$. We can then use the same scaling argument for J_{eff} that we used for J in the weak coupling regime. Incorporating the value of the effective coupling in the renormalization-group equation [cf. Eq. (1)], one can prove the perturbation J_{eff} to be irrelevant and the strong-coupling fixed point to be stable. The low-energy physics corresponds then to a system of free electrons that are weakly coupled to an effective impurity spin.

When $q>N/2$, on the contrary, $E_0^A<E_0^S$, the effective coupling is found to be antiferromagnetic, J_{eff} grows in the renormalization process, and the strong-coupling fixed point $(J=\infty)$ is unstable.

The case $q=N/2$ requires particular attention, since the leading contribution to J_{eff} vanishes. Taking into account the whole expression for the effective coupling, we find that the strong-coupling fixed point for an impurity with $q=N/2$ is stable as long as the bosonic parameter S is smaller than the critical value

$$S^*=\frac{1}{4}\left(N\sqrt{\frac{2N}{N-1}}-(N-2)\right).$$

In the large-N limit we have

$$S^*=\left(\frac{\sqrt{2}-1}{4}\right)N+\frac{4+\sqrt{2}}{8}+O(1/N)\sim\frac{N}{10}. \qquad (28)$$

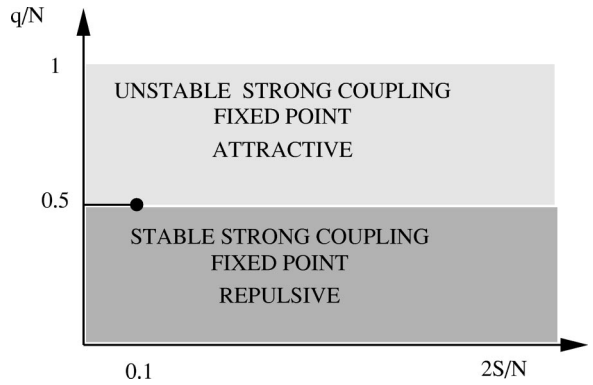

FIG. 12. Phase diagram of the model (large N, $2S/N$ finite), as a function of the impurity parameters, $2S/N$ and q/N. As soon as $q>N/2$ the strong-coupling fixed point becomes unstable. For $q=N/2$, the strong-coupling fixed point remains stable only for moderate values of $2S/N$ (short line ending in a point).

The strong-coupling fixed point at $q=N/2$ becomes unstable already at moderately large values of S. The corresponding phase diagram of the model in the large-N limit, as a function of the impurity parameters, $2S/N$ and q/N is reported in Fig. 12.

D. Sign of the effective charge interaction

In Fig. 13 we report the dependance of U_{eff} on q/N, in the large N limit. By comparisons of Eqs. (26) and (27), one can see that the change of sign of the effective interaction U_{eff} is directly connected to the change of sign of the effective coupling J_{eff} (see also Fig. 11). This result has the immediate following physical consequence. In the former regime, $q<N/2$, where the strong-coupling fixed point is stable, the effective interaction $U_{eff}>0$ is repulsive, and the lowest energy expressed in Eq. (22) is obtained for $n_d=1$. In

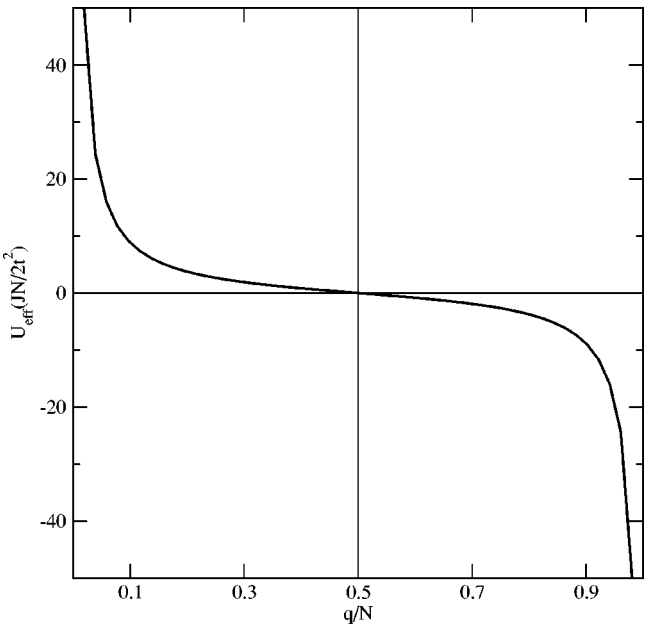

FIG. 13. Effective charge interaction U_{eff} as a function of q/N, in the large-N limit.

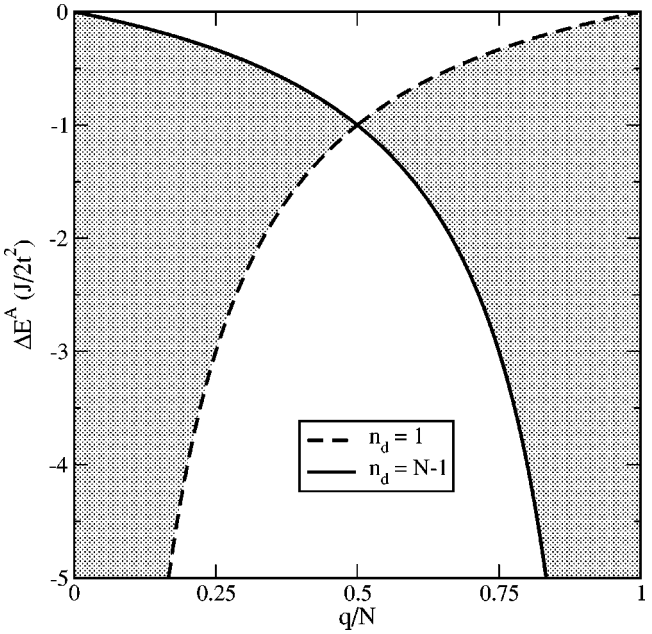

FIG. 14. Leading-order term in the energy shift, $\Delta E_0^A \sim \Delta E_0^S$, as a function of q/N, for $1<n_d<(N-1)$ (shaded region), and in the limiting cases $n_d=1$ (dashed line) and $n_d=(N-1)$ (straight line). Notice that the value at $q/N=1/2$ is equal to $-2t^2/J$, for any n_d. Note that for $q/N<0.5$ the energy is minimized for $n_d=1$, while for $q/N>0.5$ the minimization is obtained for $n_d=(N-1)$.

the latter regime, $q>N/2$, the effective interaction $U_{eff}>0$ is attractive, and the energy is minimized for $n_d=(N-1)$. We have plotted ΔE_0^A in Fig. 14. The shaded region corresponds to the possible values of ΔE_0^A for the whole range of n_d, bounded by the limiting cases, $n_d=1$ and $n_d=(N-1)$. Note that at $q=N/2$, $\Delta E_0^A(q=N/2)=-2t^2/J$ for any value of n_d.

As has been noted before, ΔE_0^A is independent of $2S$. Therefore, ΔE_0^A coincides with the energy shift for a fermionic impurity (completely antisymmetric representation) as is checked in Appendix C. When the impurity is fermionic, there is no degeneracy of the strong-coupling fixed point, which is always stable, and the lowest-order perturbation theory just shifts the ground-state energy. Nevertheless, there are two regimes, repulsive and attractive, depending on the value of q, and characterized by the value of n_d that minimizes the energy. This behavior is a consequence of the *particle-hole* symmetry in the fermionic case, given by the transformations $q\rightarrow(N-q)$ and $n_d\rightarrow(N-n_d)$ (cf. Appendix C). The behavior of a fermionic impurity with q is the same as in the case $(N-q)$, if we reinterpret the electrons as holes and the impurity as made out of holes. Therefore, if $n_d=1$ minimizes the energy for $q<N/2$ (electron repulsion), then the energy for a *hole* impurity, made out of $(N-q)$ fermions, is minimized by the state that repels the holes, $(N-n_d)=1$, implying an attraction of electrons, $n_d=(N-1)$. This behavior is shown in Fig. 15.

The addition of a bosonic component to the impurity, leading to the formation of a row in the L-shaped Young tableau representing the impurity, breaks this particle-hole symmetry. Whereas the two regimes described above are still

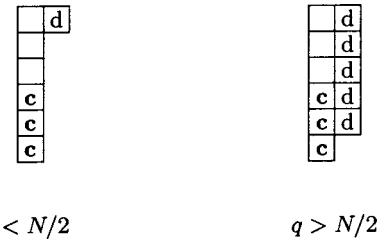

FIG. 15. Strong-coupling ground-state configurations in the fermionic case, where only hopping to the nearest-neighbor site has been included. When $q>N/2$, the impurity site attracts $N-1$ conduction electrons.

present, due to the fermionic component, the degeneracy of the states due to the bosonic component leads to the instability of the strong-coupling fixed point at the same point as where the the dressed impurity starts attracting the conduction electrons on site 1.

E. Physical properties of the model

We finish by making some remarks on the physical properties of the model in the different regimes. As is common to all models with an antiferromagnetic Kondo coupling, there will be a crossover from weak coupling above a given Kondo scale T_K to a low-energy regime. When the strong-coupling fixed point is stable, we should expect for $T\ll T_K$ a weak coupling of the effective impurity at site 0 with the rest of the electrons. The physical properties at low temperature are controlled by the degeneracy of the effective impurity, $d([2S-1])=C_{N+2S-2}^{N-1}$. Thus, we should expect a residual entropy $\mathcal{S}^i\sim\ln C_{N+2S-2}^{N-1}$ and a Curie susceptibility, $\chi^i \sim C_{N+2S-2}^{N-1}/T$, with logarithmic corrections.[41,42] This is the result that we would expect for a purely symmetric impurity. The difference with respect to the case at hand is that in the L-shaped impurity model only $(N-q)$ electrons are allowed at the origin, instead of $(N-1)$. Thus, we would expect to find different results for quantities that involve the scattering phase shift of electrons off the effective impurity. Consider, for instance, the $2S=1$ case. The phase shift δ, of the conduction electrons scattered off the impurity site, characterizes the impurity contribution to the resistivity ρ^i. At zero temperature and magnetic field, we have[30]

$$\rho^i \propto \sin^2\delta. \tag{29}$$

The phase shift for antisymmetric impurities in SU(N) was computed in Ref. 41. In the completely screened case it reads

$$e^{2i\delta}=-e^{-i\pi(1-2q/N)}. \tag{30}$$

If we choose the phase shift so that $|\delta|<\pi/2$, we have

$$\delta=\begin{cases}\pi\left(\dfrac{q}{N}\right), & q<N/2\\[2ex] -\pi\left(\dfrac{N-q}{N}\right), & q>N/2.\end{cases} \tag{31}$$

The unitary limit, $|\delta| = \pi/2$ is reached in the particle-hole symmetric case, $q = N/2$. We see that this corresponds to the point where ΔE_f is independent of n_d, indicating the change from the attractive to the repulsive regime.

In the $q > N/2$ regime, it is reasonable to think that there would be a magnetic contribution to the entropy, and a Curie-like contribution to the susceptibility, since the impurity remains unscreened. This behavior is different from that of the multichannel Kondo model, which is characterized by an intermediate coupling fixed point where the impurity magnetic degrees of freedom are completely quenched.[43] It is in the scattering properties that we might be able to see the anomalous features of this new fixed point more clearly.

V. CONCLUSIONS

In this paper, we have studied the SU(N), single-channel Kondo model, with a general impurity spin, involving both bosonic and fermionic degrees of freedom (corresponding, respectively, to the horizontal and vertical directions in a L-shaped Young tableau). This model shows a transition between two different regimes when the amount of fermionic degrees of freedom, q, becomes larger than $N/2$, in the large-N limit. The strong-coupling fixed point studied here describes the low-energy physics of the model when $q < N/2$, and it becomes unstable for $q > N/2$. We have identified the origin of this instability as related to the change, from repulsive to attractive, of the effective interaction between the dressed impurity and the conduction electrons in the neighboring sites. This change is already present in the purely fermionic case, where it happens at the particle-hole symmetry point, $q = N/2$. The only role of the bosonic degrees of freedom of the impurity is to allow for a degeneracy of the strong-coupling fixed point, which is lifted by hopping, leading to an effective spin coupling J_{eff}. The properties of this coupling, as well as the effective charge coupling, are then controlled by the fermionic component of the impurity.

We have followed a systematic approach in order to obtain the explicit form of the states needed for our calculations. As a result, our work can be used as the starting point for the study of richer systems, such as the multichannel case.

Obviously, the interesting open problem now is to fully understand the physics in the $q > N/2$ regime. This issue might have important future applications for the lattice problem, with potential consequences for the understanding of non-Fermi-liquid behavior observed in heavy-fermion systems. In order to gain some insight it would be desirable to carry out a nonperturbative study, either using NRG or Bethe ansatz techniques. Here, we would like to point out some of the limitations of these methods when applied to the model under consideration. The effects described in our work appear for $N > 5$. That is, each lattice site can be filled with up to five electrons. Furthermore, the simplest impurity that displays an intermediate fixed point corresponds to a multiplet with 45 elements. Such a large Hilbert space limits the performance of a NRG study. The difficulties of the Bethe ansatz method are of a different nature. Due to the properties of the impurity, the model with just a Kondo coupling is not integrable.[44] In the cases studied until now, the electron can couple to the impurity in two different ways: symmetrically or antisymmetrically. This leads to the usual S matrix that appears in impurity integrable models. The novelty of the impurity studied here is that the electron can couple to it in three different ways. This is an important property, and it was already noticed in Refs. 26 and 27 that it leads to the instability of the strong-coupling fixed point. However, this same property spoils integrability. Even though it is possible to construct integrable models with a spin impurity in an arbitrary representations,[45] this is done at the price of adding extra electron-impurity terms, which will likely change completely the physics of the system.

ACKNOWLEDGMENTS

The authors would like to thank N. Andrei for his continuous encouragement and discussions, and for a critical reading of this paper. We would also like to thank S. Burdin, P. Coleman, Ph. Nozières, C. Pépin, and A. Rosch for very helpful discussions. We are grateful to two different *Strongly Correlated Electron Systems* programs, held at the ICTP, Trieste, and at the Isaac Newton Institute for Mathematical Sciences, Cambridge in 2000 where this work was initiated and further developed. We would like to take this opportunity to thank the organizers for creating a stimulating environment for scientific exchange.

APPENDIX A: COMPOSITION OF THREE FUNDAMENTAL REPRESENTATIONS OF SU(3)

Before dealing with the general problem of constructing the highest weight impurity states in SU(N) in Appendix B, we will write in detail all the three-particle states with SU(3) symmetry.[38] This will allow us to see how the states constructed with different numbers of bosons and fermions can be the basis for representations with the same Young tableau. We will also see the role of the SU(3|3) and SU(1|1) supersymmetry groups induced by the realization in terms of bosons and fermions.

The direct product $\mathbf{3}\otimes\mathbf{3}\otimes\mathbf{3}$ of three fundamental representations of SU(3) gives the following Clebsh-Gordan series:

$$\mathbf{3}\otimes\mathbf{3}\otimes\mathbf{3} = (\mathbf{3}\otimes\mathbf{6})\oplus(\mathbf{3}\otimes\overline{\mathbf{3}}) = \mathbf{10}\oplus\mathbf{8}^1\oplus\mathbf{8}^2\oplus\mathbf{1}, \qquad \text{(A1)}$$

where we identify each representation by its dimension. In terms of Young tableaux, we have

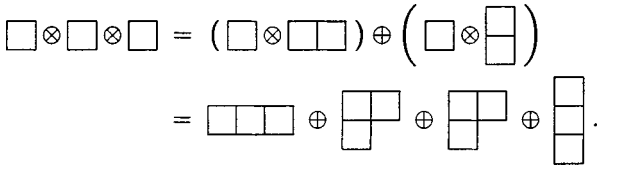

The representations $\mathbf{6}$ and $\overline{\mathbf{3}}$ result from the composition of two fundamental representations

$$\mathbf{3}\otimes\mathbf{3} = \mathbf{6}\oplus\overline{\mathbf{3}}. \qquad \text{(A2)}$$

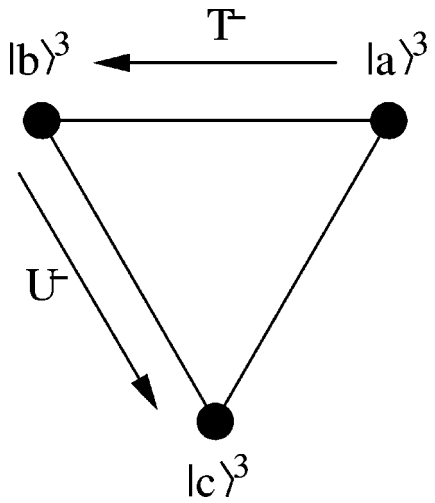

FIG. 16. Weight diagram for the fundamental representation of SU(3), with the states and the relevant lowering operators.

In addition to Young tableaux, we can use weight diagrams to describe the states in the representation, Fig. 16. In SU(3), we associate a triangle to the fundamental representation, **3**. Each vertex corresponds to a particular state of the multiplet, and the different states are related by the action of the lowering operators. In Fig. 17 we include the weight diagrams associated with Eq. (A2).

The representation **6** is completely symmetric. Its states are realized in terms of Schwinger bosons. For instance, its highest weight state can be written as

$$|aa\rangle_b^{\mathbf{6}}=\frac{1}{\sqrt{2!}}(b_a^\dagger)^2|0\rangle.$$

Here, and in the following, the values of SU(3) spin are denoted by *a*, *b*, and *c*. Likewise, the representation $\overline{\mathbf{3}}$ is completely antisymmetric, and its states are more conveniently expressed in terms of fermions. For the highest weight state, we have

$$|ab\rangle_f^{\overline{\mathbf{3}}}=f_a^\dagger f_b^\dagger|0\rangle.$$

There is another way to realize both **6** and $\overline{\mathbf{3}}$ using one boson and a fermion. Being symmetric, the highest weight of **6** is easy to write, since

$$|aa\rangle_f^{\mathbf{6}}=f_a^\dagger b_a^\dagger|0\rangle$$

is already symmetrized. To obtain the highest weight of $\overline{\mathbf{3}}$, we first have to find a state with the same quantum numbers in **6**, by acting with $T_{ab}^-=(f_b^\dagger f_a+b_b^\dagger b_a)$ on $|aa\rangle_f^{\mathbf{6}}$, to get

$$|ab\rangle_f^{\mathbf{6}}=\frac{1}{\sqrt{2}}(f_b^\dagger b_a^\dagger+f_a^\dagger b_b^\dagger)|0\rangle,$$

and find a state orthogonal to $|ab\rangle_f^{\mathbf{6}}$,

$$|ab\rangle_b^{\overline{\mathbf{3}}}=\frac{1}{\sqrt{2}}(f_b^\dagger b_a^\dagger-f_a^\dagger b_b^\dagger)|0\rangle.$$

This process is described in Fig. 17. It is easy to see that the states with the subindex *f* are related to those with the subUindex *b* by the SU(1|1) supersymmetric operator $\theta=\Sigma_a b_a^\dagger f_a$, so that $\theta|(\cdots)\rangle_f=\sqrt{2}\,|(\cdots)\rangle_b$.

Consider now the three-particle states. The easiest state to write is the highest weight state in the most symmetric representation, **10** (cf. Fig. 18),

$$|aaa\rangle^{\mathbf{10}}=|a\rangle^{\mathbf{3}}|aa\rangle^{\mathbf{6}}.$$

It can be easily expressed in terms of bosons in agreement with Eq. (B1),

$$|aaa\rangle_b^{\mathbf{10}}=\frac{1}{\sqrt{3!}}(b_a^\dagger)^3|0\rangle.$$

Alternatively, we can use a realization with two bosons (from **6**) and a fermion (from **3**),

$$|aaa\rangle_f^{\mathbf{10}}=\frac{1}{\sqrt{2!}}f_a^\dagger(b_a^\dagger)^2|0\rangle.$$

Other states of the representation are obtained by the repeated action of lowering operators. For instance,

$$|aab\rangle^{\mathbf{10}}=\frac{1}{\sqrt{3}}(\sqrt{2}|a\rangle^{\mathbf{3}}|ab\rangle^{\mathbf{6}}+|b\rangle^{\mathbf{3}}|aa\rangle^{\mathbf{6}}), \qquad \text{(A3)}$$

which leads to

$$|aab\rangle_b^{\mathbf{10}}=\frac{1}{\sqrt{2!}}(b_a^\dagger)^2b_b^\dagger|0\rangle,$$

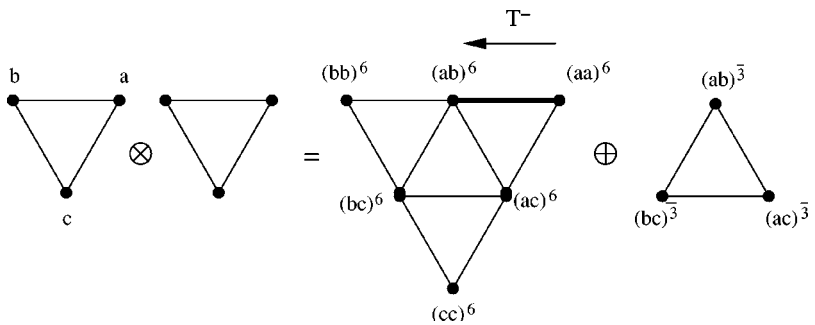

FIG. 17. Weight diagram for the Clebsch-Gordan series of the product of two fundamental representations of SU(3).

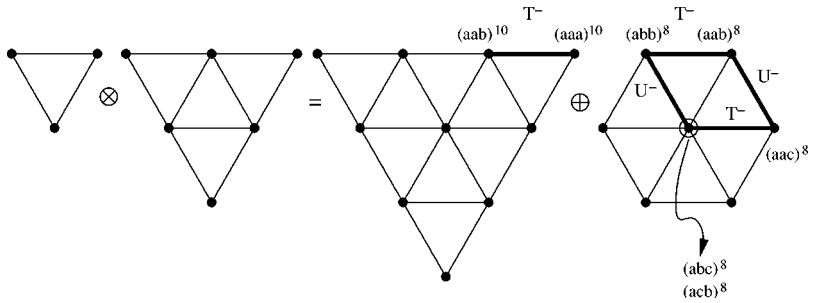

FIG. 18. Weight diagram for the Clebsch-Gordan series of the product $\mathbf{3}\otimes\mathbf{6}$. We indicate some of the states and outline the process of obtaining Clebsch-Gordan coefficients.

$$|aab\rangle_f^{\mathbf{10}}=\frac{1}{\sqrt{6}}[2f_a^\dagger b_a^\dagger b_b^\dagger+f_b^\dagger(b_a^\dagger)^2].$$

The octets, **8** are mixed symmetry representations that have to be built by a combination of fermions and bosons. The Clebsch-Gordan series (A1) indicates that $\mathbf{8}^1$, built from the product $\mathbf{3}\otimes\mathbf{6}$ is naturally realized by states with one fermion and two bosons, Fig. 18, whereas $\mathbf{8}^2$ is realized by the product of one boson and two fermions ($\mathbf{3}\otimes\overline{\mathbf{3}}$), Fig. 19. The highest weight state, $|aab\rangle^{\mathbf{8}^1}$, of the octet $\mathbf{8}^1$ is orthogonal to $|aab\rangle^{\mathbf{10}}$ defined in Eq. (A3),

$$|aab\rangle_b^{\mathbf{8}^1}=\frac{1}{\sqrt{3}}(|a\rangle^{\mathbf{3}}|ab\rangle^{\mathbf{6}}-\sqrt{2}|b\rangle^{\mathbf{3}}|aa\rangle^{\mathbf{6}})$$

$$=\frac{1}{\sqrt{3}}b_a^\dagger(f_a^\dagger b_b^\dagger-f_a^\dagger b_b^\dagger)|0\rangle,$$

in agreement with the general expression of the state ψ_b given in Eq. (B3).

As usual, the other states of the octet are built by the repeated action of generators $T^-=(f_b^\dagger f_a+b_b^\dagger b_a)$, $U^-=(f_b^\dagger f_c+b_b^\dagger b_c)$, and $V^-=(f_a^\dagger f_c+b_a^\dagger b_c)$, of SU(3). For instance,

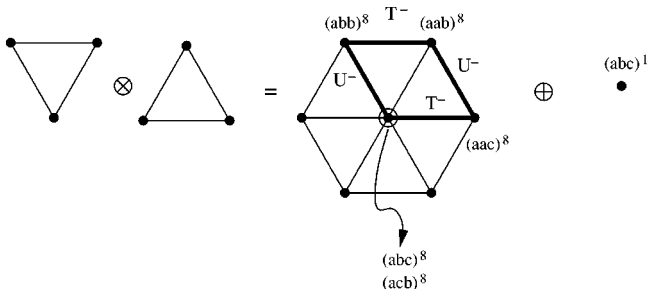

FIG. 19. Weight diagram for the Clebsch-Gordan series of the product $\mathbf{3}\otimes\overline{\mathbf{6}}$.

$$|abc\rangle_b^{\mathbf{8}^1}=\frac{1}{\sqrt{2}}T^-|aac\rangle^{\mathbf{8}^1}$$

$$=\frac{1}{\sqrt{6}}(|a\rangle^{\mathbf{3}}|bc\rangle^{\mathbf{6}}+|b\rangle^{\mathbf{3}}|ac\rangle^{\mathbf{6}}-2|c\rangle^{\mathbf{3}}|ab\rangle^{\mathbf{6}})$$

$$=\frac{1}{\sqrt{6}}(f_a^\dagger b_b^\dagger b_c^\dagger+f_b^\dagger b_a^\dagger b_c^\dagger-2f_c^\dagger b_a^\dagger b_b^\dagger)|0\rangle.$$

This state is degenerate, since there is another state in the multiplet with the same quantum numbers. In order to find this last state, $|acb\rangle^{\mathbf{8}^1}$, we have to combine the action of lowering operators with orthogonality with respect to $|abc\rangle^{\mathbf{8}^1}$. Acting with U^- on $|abb\rangle^{\mathbf{8}^1}$ leads to a state that is not orthogonal to $|abc\rangle^{\mathbf{8}^1}$. Therefore, we write

$$U^-|abb\rangle^{\mathbf{8}^1}=\sqrt{2}(\alpha\,|abc\rangle^{\mathbf{8}^1}+\beta\,|acb\rangle^{\mathbf{8}^1}).$$

There are two ways of reaching states with quantum numbers $\{abc\}$ starting from $|aab\rangle^{\mathbf{8}^1}$. We use this and the fact that $[T^+,U^-]=0$, $[T^+=(T^-)^\dagger]$, to derive α,

$$2\alpha=\sqrt{2}{}^{\mathbf{8}^1}\langle abc|U^-|abb\rangle^{\mathbf{8}^1}={}^{\mathbf{8}^1}\langle aac|T^+U^-T^-|aab\rangle^{\mathbf{8}^1}$$
$$={}^{\mathbf{8}^1}\langle aab|U^+T^+U^-T^-|aab\rangle^{\mathbf{8}^1}$$
$$={}^{\mathbf{8}^1}\langle aab|T^+T^-U^+U^-|aab\rangle^{\mathbf{8}^1}=1.$$

Hence one deduces $\alpha=1/2$ and $\beta=\sqrt{3}/2$ and one gets the expression of the last state $|acb\rangle_b^{\mathbf{8}^1}$ of the octet

$$|acb\rangle_b^{\mathbf{8}^1}=\frac{1}{\sqrt{2}}(|a\rangle^{\mathbf{3}}|bc\rangle^{\mathbf{6}}-|b\rangle^{\mathbf{3}}|ac\rangle^{\mathbf{6}})$$

$$=\frac{1}{\sqrt{2}}(f_a^\dagger b_b^\dagger b_c^\dagger-f_b^\dagger b_a^\dagger b_c^\dagger)|0\rangle.$$

To summarize, the rule is to describe the highest weight state of the octet $|aab\rangle_b$ using the bosonic representation, ψ_b, and hence to derive the other states of the octet by the above construction allowing to recover the Clebsch-Gordan coefficients involved in the spin composition related to the direct product $3\otimes 6$.

The highest weight state of the octet $\mathbf{8}^2$ is also the highest weight state of $\mathbf{3}\otimes\overline{\mathbf{3}}$,

$$|aab\rangle_f^{\mathbf{8}^2}=|a\rangle^{\mathbf{3}}|ab\rangle^{\overline{\mathbf{3}}}=b_a^\dagger f_a^\dagger f_b^\dagger|0\rangle,$$

in agreement with the general expression of the state ψ_f, Eq. (B4). The construction of the other states follow the same lines as in the case of the $\mathbf{8}^1$ octet. For instance,

$$|abc\rangle_f^{\mathbf{8}^2}=\frac{1}{\sqrt{2}}(|a\rangle^{\mathbf{3}}|bc\rangle^{\overline{\mathbf{3}}}-|b\rangle^{\mathbf{3}}|ca\rangle^{\overline{\mathbf{3}}})$$

$$=\frac{1}{\sqrt{2}}(b_a^\dagger f_b^\dagger f_c^\dagger-b_b^\dagger f_c^\dagger f_a^\dagger)|0\rangle,$$

$$|acb\rangle_f^{\mathbf{8}^2}=\frac{1}{\sqrt{6}}(|a\rangle^{\mathbf{3}}|bc\rangle^{\overline{\mathbf{3}}}+|b\rangle^{\mathbf{3}}|ca\rangle^{\overline{\mathbf{3}}}-2|c\rangle^{\mathbf{3}}|ab\rangle^{\overline{\mathbf{3}}})$$

$$=\frac{1}{\sqrt{6}}(b_a^\dagger f_b^\dagger f_c^\dagger+b_b^\dagger f_c^\dagger f_a^\dagger-2b_c^\dagger f_a^\dagger f_b^\dagger)|0\rangle.$$

Once again, the two basis of states corresponding to the same Young tableau, are related by the SU(1|1) operators, $\theta^\dagger$ and θ.

Finally, the singlet state $|abc\rangle^{\mathbf{1}}$ is built by orthogonality with the states $|abc\rangle^{\mathbf{8}^2}$, and $|acb\rangle^{\mathbf{8}^2}$, from the octet in the product $\mathbf{3}\otimes\overline{\mathbf{3}}$ (Fig. 19),

$$|abc\rangle^{\mathbf{1}}=\frac{1}{\sqrt{3}}(|a\rangle^{\mathbf{3}}|bc\rangle^{\overline{\mathbf{3}}}+|b\rangle^{\mathbf{3}}|ca\rangle^{\overline{\mathbf{3}}}+|c\rangle^{\mathbf{3}}|ab\rangle^{\overline{\mathbf{3}}}),\quad\text{(A4)}$$

in agreement with the expression of the states in the completely antisymmetric representation of the spin (B2). The simplest way to realize this state is with three fermions. Then

$$|abc\rangle_f^{\mathbf{1}}=f_a^\dagger f_b^\dagger f_c^\dagger|0\rangle.\quad\text{(A5)}$$

But it can also be written with one boson and two fermions, either by acting with θ on Eq. (A5) or by substituting on Eq. (A4),

$$|abc\rangle_b^{\mathbf{1}}=\frac{1}{\sqrt{3}}(b_a^\dagger f_b^\dagger f_c^\dagger+b_b^\dagger f_c^\dagger f_a^\dagger+b_c^\dagger f_a^\dagger f_b^\dagger)|0\rangle.$$

We have shown how to construct the states for different representations of SU(3). These results can be summarized as tables of Clebsch-Gordan coefficients like the ones that we presented in Tables IV–VII for SU(N).

Let us make some comments about the number of states. The direct product of three fundamental representations of SU(3) generates a space of dimension 27, which breaks down as a direct sum of irreducible representations according to the Clebsch-Gordan series (A1). By considering all the realizations of these states in terms of bosons and fermions subject only to the constraint $Q=n_f+n_b=3$, we are working on the higher dimensional space of a representation of SU(3|3) with a total of 38 states, as represented in Fig. 20. The figure also reports the relation between these states with

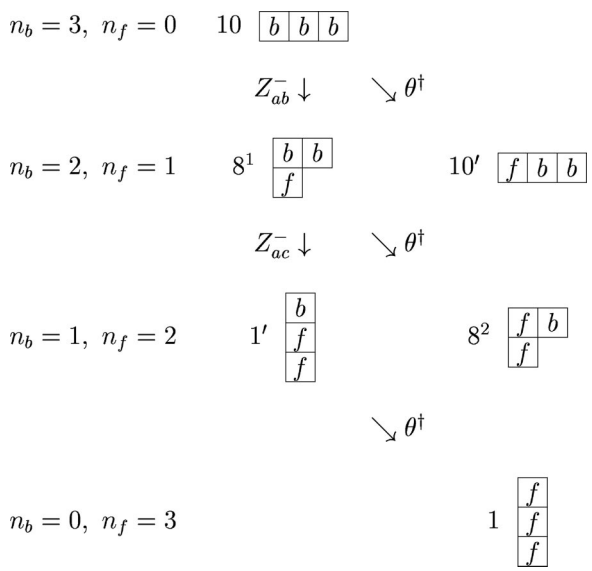

FIG. 20. States with $Q=(n_b+n_f)$ grouped according to SU(3) representations.

the introduction of an additional supersymmetric operator, $Z_{ar_q}^-=f_{r_q}^\dagger b_a$, acting on the highest weight states. The states **10** and **10**′, respectively, are identical (as well as **1** and **1**′) as far as the SU(3) symmetry is concerned. This is not the case of the two states $\mathbf{8}^1$ and $\mathbf{8}^2$, which correspond to different spin representations even if the associated Young tableaux are the same. Altogether, one recovers the expected total of 27 different states.

APPENDIX B: IMPURITY STATES AND LOW-LYING STATES IN THE STRONG-COUPLING LIMIT

We present in this appendix the explicit form of the highest weight (spin) states for the impurity and for the low-lying states in the $J\to\infty$ limit. We discuss in detail the use of Young tableaux both to describe the symmetry properties of the states and to study the SU(N) generalization of the composition of several spins.

1. Impurity state

Before studying the general case of a L-shaped Young tableau representation of spin, we will consider the two limiting cases of a completely symmetric (bosonic) and an antisymmetric (fermionic) representation of the spin in SU(N).

The case of a completely symmetric representation of the spin is equivalent to a system of $2S$ identical particles symmetric under the permutation of two of them. The associated Young tableau is made of a single line of $2S$ boxes

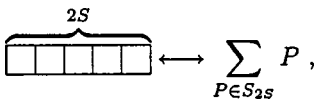

$$\longleftrightarrow\ \sum_{P\in S_{2S}} P\ ,$$

expressed in shorthand notation as $[2S]$. Associated with the Young tableau, there is a symmetrizer operator made out of the sum of all the permutations of $2S$ elements. It is convenient to use an explicit representation of the localized spin in

terms of N species of Schwinger bosons (see, for instance, Ref. 46), b_α ($\alpha=a,b,\ldots,r_N$) subject to the constraint

$$\hat{n}_b=\sum_\alpha b_\alpha^\dagger b_\alpha=2S.$$

The (N^2-1) components of the spin operator can be represented as $\mathbf{S}^A=\Sigma_{\alpha\beta}b_\alpha^\dagger \boldsymbol{\tau}_{\alpha\beta}b_\beta$, while the highest weight state [the analog of the state with the largest value of S^z in SU(2)], can be written as

$$|(a)^{2S}\rangle^{[2S]}=\frac{1}{\sqrt{(2S)!}}(b_a^\dagger)^{2S}|0\rangle, \tag{B1}$$

where $|0\rangle$ denotes the vacuum state for the bosons. Other states of the representation can be obtained from this one by the repeated action of lowering operators, taking advantage of the underlying SU(2) subalgebras within SU(N). Take, for instance, the $(2S+1)$ states $\{|(a)^x(b)^y\rangle^{[2S]}\}$ with $x+y=2S$. They transform as a regular, SU(2), spin-S multiplet under the action of the SU(N) operators $T_{ab}^-=b_b^\dagger b_a$, $T_{ab}^+=b_a^\dagger b_b$, and $T_{ab}^z=(b_a^\dagger b_a-b_b^\dagger b_b)/2$. In particular,

$$T_{ab}^-\,|a^{2S}\rangle^{[2S]}=\sqrt{2S}\;|(a)^{2S-1}b\rangle^{[2S]},$$

or, in terms of bosons,

$$|(a)^{2S-1}b\rangle^{[2S]}=\frac{1}{\sqrt{(2S-1)!}}(b_a^\dagger)^{(2S-1)}b_b^\dagger|0\rangle.$$

Note that each index in the set of quantum numbers, $\{\alpha,\beta\ldots,\rho_{2S}\}$, describing the states of the representation, can take N values independently of the rest of the set, and that for each set of values there is only one state. The dimension of the representation is thus given by C_{N+2S-1}^{2S}, corresponding to the number of ways of choosing $2S$ elements out of a group of $(N+2S-1)$.

The other limiting case corresponds to a completely antisymmetric representation of the spin. It is equivalent to the case of q identical particles antisymmetric under the permutation of two of them. The associated Young tableau is made out of a single column of q boxes,

$$q\left\{\begin{array}{|c|}\hline\\\hline\\\hline\\\hline\\\hline\end{array}\right. \longleftrightarrow \sum_{P\in S_q}\delta_P P\ ,$$

and expressed in shorthand notation as $[1^q]$ with $q<N$. Associated with the Young tableau, there is an antisymmetrizer operator made out of the sum of all the permutations of q elements weighted by a $\delta_P=\pm 1$ factor as for antisymmetric identical particles. It is convenient to use an explicit representation of the localized spin in terms of N species of Abrikosov pseudofermions[47] f_α ($\alpha=a,b,\ldots,r_N$) subject to the constraint

$$\hat{n}_f=\sum_\alpha f_\alpha^\dagger f_\alpha=q.$$

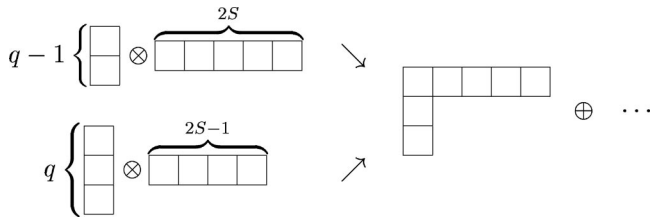

FIG. 21. Two ways of obtaining a L-shaped representation out of the direct product of a symmetric and an antisymmetric SU(N) representation.

The generators of SU(N) in this realization are $\mathbf{S}^A=\Sigma_{\alpha\beta}f_\alpha^\dagger \boldsymbol{\tau}_{\alpha\beta}^A f_\beta$, and the highest weight state of the representation can be written as

$$|ab\cdots r_q\rangle^{[1^q]}=f_a^\dagger f_b^\dagger\cdots f_{r_q}^\dagger|0\rangle \tag{B2}$$

involving a set $\{a,b,\ldots,r_q\}$ of q different indices. Other states of the representation can be obtained from this one by the repeated action of lowering operators such as $T_{ab}^-=f_b^\dagger f_a$, taking advantage of the underlying SU(2) subalgebras. Note that the states are SU(2) doublets with respect to these subalgebras. The dimension of the representation is given by C_N^q.

An important property of both kinds of representations is that the states are nondegenerate. That is, each set of allowed quantum numbers completely determine the state. This is not the case for mixed symmetry representations, as we are about to see.

Let us now consider the general L-shaped representation of spin, Fig. 1, which interpolates between the previous two limits. Its dimension can be easily obtained using Robinson's formula:[48] the result is $[2S/(2S+q-1)]C_{N+2S-1}^{2S}C_{N-1}^{q-1}$ (Table IV). The L-shaped representation is the result of the direct product of a symmetric and an antisymmetric representation. This can be done in two nonequivalent ways (Fig. 21) : either as the $[1^{q-1}]\otimes[2S]\rightarrow[2S,1^{q-1}]\oplus\cdots$ Clebsch-Gordan series, or as $[1^q]\otimes[2S-1]\rightarrow[2S,1^{q-1}]\oplus\cdots$. The construction of the highest weight states for each of the cases is detailed at the end of this subsection [cf. Eqs. (B9) and (B12)] and leads to

$$\begin{aligned}\psi_b&=|(a)^{2S}b\cdots r_q\rangle^{[2S,1^{q-1}]}\\&=\frac{1}{\sqrt{2S+q-1}}\frac{(b_a^\dagger)^{2S-1}}{\sqrt{(2S-1)!}}\mathcal{A}(b_a^\dagger f_b^\dagger f_c^\dagger\cdots f_{r_q}^\dagger)|0\rangle\end{aligned} \tag{B3}$$

and

$$\psi_f=|(a)^{2S}b\cdots r_q\rangle^{[2S,1^{q-1}]}=\frac{(b_a^\dagger)^{2S-1}}{\sqrt{(2S-1)!}}(f_a^\dagger f_b^\dagger f_c^\dagger\cdots f_{r_q}^\dagger)|0\rangle, \tag{B4}$$

where $\mathcal{A}(\cdots)$ is the antisymmetrizer. The impurity spin operator has a form that is independent of either $2S$ or q and is given by $S=\Sigma_{\alpha\beta}(b_\alpha^\dagger \boldsymbol{\tau}_{\alpha\beta}b_\beta+f_\alpha^\dagger \boldsymbol{\tau}_{\alpha\beta}f_\beta)$. The first constraint has to do with the conservation of the number of particles

$$\hat{Q}=(\hat{n}_f+\hat{n}_b)=(2S+q-1), \tag{B5}$$

where $(2S+q-1)$ denotes the number of boxes in the L-shaped Young tableau. In the limiting cases discussed previously, once the value of Q is fixed, the representation is completely determined. Here, however, it is necessary to add a second constraint to identify states with the right symmetry. To that end, it is worth noticing that the set of states ψ_b and ψ_f form a basis for a representation of the larger, supersymmetric group SU($N|N$), with generators given as linear combinations of the operators $b_\alpha^\dagger b_\beta$, $f_\alpha^\dagger f_\beta$, $b_\alpha^\dagger f_\beta$, $f_\alpha^\dagger b_\beta$. Thus, all the L-shaped impurities that interpolate between the symmetric and the antisymmetric case are related by the supersymmetric group. As a matter of fact, the constraints that fix the SU(N) representation are obtained from operators in SU($N|N$) diagonal in spin, such as $\hat{n}_f$, $\hat{n}_b$, $\theta=\Sigma_\alpha b_\alpha^\dagger f_\alpha$, and $\theta^\dagger$. Consider, for instance, the action of $\theta^\dagger$ on ψ_b,

$$\theta^\dagger (b_a^\dagger)^{2S-1}\mathcal{A}(b_a^\dagger f_b^\dagger f_c^\dagger\cdots f_{r_q}^\dagger)\ |0\rangle$$
$$=(2S+q-1)(b_a^\dagger)^{2S-1}(f_a^\dagger f_b^\dagger f_c^\dagger\cdots f_{r_q}^\dagger)|0\rangle,$$

where the right-hand side corresponds to ψ_f. This leads to the relations

$$\theta^\dagger\psi_b=\sqrt{2S+q-1}\ \ \psi_f,$$

$$\theta\ \ \psi_f=\sqrt{2S+q-1}\ \ \psi_b.$$

Notice also that $\theta^\dagger\psi_f=\theta\psi_b=0$. The operators θ and $\theta^\dagger$ relate states that transform under a representation of SU(N) given by the same Young tableau. Together with $\hat{Q}$, they form the SU($1|1$) supersymmetric algebra[26] $\{\theta,\theta^\dagger\}=\hat{Q}$. Furthermore, the operators $P_b=(1/Q)\theta\theta^\dagger$ and $P_f=(1/Q)\theta^\dagger\theta$ are the projectors out of the bosonic ψ_b and the fermionic ψ_f states, respectively. The states ψ_f and ψ_b are the exact analog of the familiar example of the formation of the two octets, $\mathbf{8}^1$ and $\mathbf{8}^2$, out of the composition of three fundamental representations in SU(3). In Appendix A we construct the states explicitely in this example and derive the corresponding Clebsch-Gordan coefficients.

The second constraint is then given by $\hat{\mathcal{Y}}$, a bilinear combination of the operators $\{\hat{n}_f,\hat{n}_b,\theta,\theta^\dagger\}$ since it is a consequence of the invariance of the Casimir operator $\hat{\mathcal{C}}_2$ [the SU(N) generalization of $\mathbf{S}^2=S(S+1)$], which for a L-shaped representation is given by

$$\mathcal{C}_2(\hat{R})=\sum_A \mathbf{S}^A\cdot\mathbf{S}^A=\frac{1}{2}\left[\hat{Q}\left(N-\frac{\hat{Q}}{N}\right)-\hat{\mathcal{Y}}\right]. \tag{B6}$$

Here, $\hat{\mathcal{Y}}=\hat{Q}(\hat{n}_f-\hat{n}_b)+[\theta,\theta^\dagger]$. Once the first constraint, Eq. (B5) is fulfilled, the invariance of the Casimir $\hat{\mathcal{C}}_2$ is ensured provided that the operator $\hat{\mathcal{Y}}$ is invariant too. This leads to the second constraint

$$\hat{\mathcal{Y}}=Q(q-2S). \tag{B7}$$

It is easy to check that the operators θ and $\theta^\dagger$ commute with $\hat{Q}$ and $\hat{\mathcal{Y}}$, which implies that the constraints are also compatible with the SU($1|1$) supersymmetry. Note that this was not the case for the operator $\hat{\mathcal{Y}}'=\hat{n}_f-\hat{n}_b+(1/Q)[\theta,\theta^\dagger]$ defined in Eq. (10) of Ref. 26.

The constraints completely determine the representation, but they cannot distinguish between the states ψ_f and ψ_b. The physical properties of the system depend only on the Young tableau associated with the Kondo impurity, and not on the particular way the representation basis is constructed.

We finish this section by describing in detail the construction of the relevant states of the impurity multiplet.

The direct product of irreducible representations of SU(N) decomposes into a direct sum of irreducible representations (Clebsch-Gordan series). A well-known example is the addition of angular momentum in SU(2). In order to find the states in the new basis [leading to the Clebsch-Gordan coefficients (CGC)], we follow a similar procedure to the one used for angular momentum (see also Appendix A). That is, we first identify the highest weight state of the product of representations, which is always nondegenerate, with the highest weight state of the most *symmetric* of the representations in the Clebsch-Gordan series. Then, we use lowering operators [particular combinations of the generators of SU(N)] to generate other states in the same representation. For arbitrary N there might be more than one state with the same quantum numbers in the same representation [as in the SU(3) octet, $\mathbf{8}^1$ and $\mathbf{8}^2$], and we will have to find orthogonal combinations. Finally, we find states in the next representation by looking for additional orthogonal states with the same quantum numbers, and acting on them with lowering operators.

The direct product of a symmetric and an antisymmetric representation of SU(N) can be expressed as a direct sum of two L-shaped representations, according to the Clebsh-Gordan series

$$[2S-1]\ \otimes\ [1^q]\ =\ [2S,1^{q-1}]\ \oplus\ [2S-1,1^q]$$

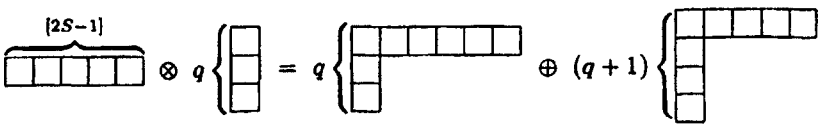

with dimensions

$$C^{2S-1}_{N+2S-2}\ C^{q}_{N}=\frac{2S}{2S+q-1}\ C^{2S}_{N+2S-1}\ C^{q-1}_{N-1}+\frac{2S-1}{2S+q-1}\ C^{2S-1}_{N+2S-2}\ C^{q}_{N-1}.$$

We proceed now to write the states in each L-shaped representation. The *most symmetric* (highest weight state) of the product $[2S-1]\otimes[1^q]$ is

$$|(a)^{2S-1}\rangle^{[2S-1]}|abc\cdots r_q\rangle^{[1^q]},$$

where $2S$ particles have the same quantum number a. This state is also the highest weight state of the most symmetric of the representations, $[2S,1^{q-1}]$,

$$|(a)^{2S}bc\cdots r_q\rangle^{[2S,1^{q-1}]}=|(a)^{2S-1}\rangle^{[2S-1]}|abc\cdots r_q\rangle^{[1^q]}. \tag{B8}$$

Notice that the lowering operators that transform the value a into $\delta\in[b,r_q]$ affect the $[2S-1]$ state only, since the $[1^q]$ term is completely antisymmetric. Thus, these states are also nondegenerate

$$|(a)^{2S-1}bc\cdots(\delta)^2\cdots r_q\rangle^{[2S,1^{q-1}]}=|(a)^{2S-2}\delta\rangle^{[2S-1]}|abc\cdots r_q\rangle^{[1^q]}. \tag{B9}$$

Other states with $2S$ of the α_j equal to a, can be obtained from Eq. (B8). They are also nondegenerate. For instance the state with the value γ replaced by r_{q+1} is

$$|(a)^{2S}bcd\cdots r_q r_{q+1}(no\ \ \gamma)\rangle^{[2S,1^{q-1}]}=|(a)^{2S-1}\rangle^{[2S-1]}|abcd\cdots r_q r_{q+1}(no\ \ \gamma)\rangle^{[1^q]}. \tag{B10}$$

Altogether, there are q states of this type (if we restrict the α_j to the range $[a,r_{q+1}]$).

Next, we construct the states in $[2S,1^{q-1}]$ where $(2S-1)$ of the α_j are equal to a and the rest of labels are different and take values in the range $[b,r_{q+1}]$. There are q linearly independent states of this kind. For instance, acting with T^-_{ac} on (B10) we get

$$\begin{aligned}T^-_{ac}|(a)^{2S}bcd\cdots r_q r_{q+1}(no\ \ \gamma)\rangle^{[2S,1^{q-1}]}&=\sqrt{2S}\ \ |(a)^{2S-1}bcd\cdots r_q r_{q+1}\rangle^{[2S,1^{q-1}]}\\&=\sqrt{2S-1}\ \ |(a)^{2S-2}\gamma\rangle^{[2S-1]}|abc\cdots r_q r_{q+1}(no\ \ \gamma)\rangle^{[1^q]}\\&\quad+|(a)^{2S-1}\rangle^{[2S-1]}|bcd\cdots r_q r_{q+1}\rangle^{[1^q]}.\end{aligned} \tag{B11}$$

The orthogonalization of these q states leads to the first q rows of Table VII of CGC. The last line in the table correspond to a state with the same quantum numbers $((a)^{2S-1}bcd\cdots r_q r_{q+1})$, and orthogonal to all the states in $[2S,1^q]$. This state is the highest weight of $[2S-1,1^q]$. It is easy to see that it must be of the form

$$\begin{aligned}|(a)^{2S-1}bcd\cdots r_q r_{q+1}\rangle^{[2S-1,1^q]}&=\frac{1}{\sqrt{2S+q-1}}\Bigg[\sqrt{2S-1}\ |(a)^{2S-1}\rangle^{[2S-1]}|bcd\cdots r_q\rangle^{[1^q]}\\&\quad+\sum_{\beta=b}^{r_q}(-1)^{\delta_{a\beta}}|(a)^{2S-2}\beta\rangle^{[2S-1]}\\&\quad\times|bc\cdots r_q(no\ \ \beta)\rangle^{[1^q]}\Bigg].\end{aligned} \tag{B12}$$

2. Ground state

The explicit form of the highest weight state for the ground state corresponds to Eq. (5),

$$|\mathrm{GS}\rangle^{[2S-1]}_{\{a\}aa}=\frac{1}{\sqrt{(2S-1)!}}(b^\dagger_a)^{2S-1}|\Delta\rangle,$$

with

$$|\Delta\rangle\equiv\frac{1}{\gamma}\mathcal{A}\left[b^\dagger_{i_1}\left(\prod_{\alpha=i_2}^{i_q}f^\dagger_\alpha\right)\left(\prod_{\beta=i_{q+1}}^{i_N}c^\dagger_\beta\right)\right]|0\rangle,$$

$$\gamma\equiv\sqrt{(2S+N-1)C^{q-1}_{N-1}}.$$

Notice the additional term C^{q-1}_{N-1} in the normalization factor γ, as compared to Eq. (B3), due to the presence of two kinds of fermions, $f^\dagger_\alpha$ and $c^\dagger_\alpha$. We adopt the bosonic realization of the impurity ψ_b, which simplifies the calculations. We would like to emphasize that all the results are independent of the realization chosen, since only the form of the Young tableau is relevant to the interaction.

Other states in the same $[2S-1]$ multiplet can be obtained by just acting on the $(b^\dagger_a)^{2S-1}$ term. For instance,

$$T^-\ \ |\mathrm{GS}\rangle_{\{a\}aa}=\sqrt{2S-1}\ \ |\mathrm{GS}\rangle_{\{a\}ab}=(2S-1)\frac{1}{\sqrt{(2S-1)!}}\ b^\dagger_b(b^\dagger_a)^{2S-2}|\Delta\rangle, \tag{B13}$$

$$U^-\ \ |\mathrm{GS}\rangle_{\{a\}ab}=|\mathrm{GS}\rangle_{\{a\}ac}=\frac{1}{\sqrt{(2S-2)!}}\ b^\dagger_c(b^\dagger_a)^{2S-2}|\Delta\rangle, \tag{B14}$$

and

$$|\mathrm{GS}\rangle_{\{a\}ab}=\frac{1}{\sqrt{(2S-2)!}}b^\dagger_b(b^\dagger_a)^{2S-2}|\Delta\rangle,$$

$$|\mathrm{GS}\rangle_{\{a\}bb}=\frac{1}{\sqrt{2(2S-3)!}}(b^\dagger_b)^2(b^\dagger_a)^{2S-3}|\Delta\rangle,$$

$$|\mathrm{GS}\rangle_{\{a\}ac}=\frac{1}{\sqrt{(2S-2)!}}b^\dagger_c(b^\dagger_a)^{2S-2}|\Delta\rangle,$$

$$|\mathrm{GS}\rangle_{\{a\}bc}=\frac{1}{\sqrt{(2S-3)!}}b_b^\dagger b_c^\dagger (b_a^\dagger)^{2S-3}|\Delta\rangle. \quad \text{(B15)}$$

3. Excited states

Let us now write the expression of the excited states of the strong-coupling fixed point. The states in $|\mathrm{GS}+1\rangle^S$ transform as the completely symmetric representation $[2S]$. The highest weight state can be obtained by acting with $c_a^\dagger$ on the ground state,

$$|\mathrm{GS}+1\rangle^S_{\{a\}aaa}=\frac{1}{\Omega}c_a^\dagger|\mathrm{GS}\rangle_{\{a\}aa},$$

where the normalization factor, $\Omega=\sqrt{2S+q-1/(2S+N-1)}$, appears[27] because the additional c electron has to be antisymmetrized with respect to the $(N-q)$ electrons already present on site 0. Other states in the multiplet can be obtained by repeated action of the lowering operators, as in Eqs. (B13) and (B15). For instance,

$$|\mathrm{GS}+1\rangle^S_{\{a\}aab}=\frac{1}{\Omega}\frac{1}{\sqrt{2S}}[\sqrt{2S-1}c_a^\dagger|\mathrm{GS}\rangle_{\{a\}ab}+c_b^\dagger|\mathrm{GS}\rangle_{\{a\}aa}], \quad \text{(B16)}$$

$$|\mathrm{GS}+1\rangle^S_{\{a\}abc}=\frac{1}{\Omega}\frac{1}{\sqrt{2S}}[\sqrt{2S-2}c_a^\dagger|\mathrm{GS}\rangle_{\{a\}bc}+c_b^\dagger|\mathrm{GS}\rangle_{\{a\}ac}+c_c^\dagger|\mathrm{GS}\rangle_{\{a\}ab}].$$

States in $|\mathrm{GS}+1\rangle^A$ transform as $[2S-1,1]$. The highest weight state is $|\mathrm{GS}+1\rangle^A_{\{a\}aab}$, and it will be orthogonal to the state defined in Eq. (B16). Thus,

$$|\mathrm{GS}+1\rangle^A_{\{a\}aab}=\frac{1}{\Lambda}\frac{1}{\sqrt{2S}}[c_a^\dagger|\mathrm{GS}\rangle_{\{a\}ab}-\sqrt{2S-1}c_b^\dagger|\mathrm{GS}\rangle_{\{a\}aa}],$$

with[27] $\Lambda=\sqrt{(q-1)/(N-1)}$. Notice the difference with respect to the normalization factor. Only Ω depends on $2S$.

Other states in $|\mathrm{GS}+1\rangle^A$ are obtained in a very similar way to the construction of the octets, $\mathbf{8}^1$ and $\mathbf{8}^2$ in SU(3) (see Appendix A). For instance,

$$|\mathrm{GS}+1\rangle^A_{\{a\}abc}=\frac{1}{\Lambda}\frac{1}{\sqrt{2S(2S-1)}}[\sqrt{2S-2}c_a^\dagger|\mathrm{GS}\rangle_{bc}+c_b^\dagger|\mathrm{GS}\rangle_{ac}-(2S-1)c_c^\dagger|\mathrm{GS}\rangle_{ab}],$$

$$|\mathrm{GS}+1\rangle^A_{\{a\}acb}=\frac{1}{\Lambda}\frac{1}{\sqrt{2S-1}}[c_a^\dagger|\mathrm{GS}\rangle_{bc}-\sqrt{2S-2}c_b^\dagger|\mathrm{GS}\rangle_{ac}].$$

We collect the coefficients for the states with quantum numbers $\{\{a\}abc\}$ in Table III, which shows Clebsch-Gordan coefficients corresponding to the direct product $[1]\otimes[2S-1]$ in SU(N), following the notation of Ref. 49.

TABLE III. Clebsch-Gordan coefficients for the excited states with one additional electron, corresponding to the product $[1]\otimes[2S-1]$, and to states with quantum nubers $\{\{a\}abc\}$. The normalization factor is $1\sqrt{N}$, and a $\sqrt{}$ is understood over each coefficient (Ref. 49). The minus sign indicates a negative sign in from of the square root, $-\sqrt{}$.

	N	$c_a^\dagger\|\mathrm{GS}\rangle_{\{a\}bc}$	$c_b^\dagger\|\mathrm{GS}\rangle_{\{a\}ac}$	$c_c^\dagger\|\mathrm{GS}\rangle_{\{a\}ab}$
$\Omega\|\mathrm{GS}+1\rangle^S_{\{a\}abc}$	$2S$	$2S-2$	1	1
$\Lambda\|\mathrm{GS}+1\rangle^A_{\{a\}abc}$	$2S(2S-1)$	$2S-2$	1	$-(2S-1)^2$
$\Lambda\|\mathrm{GS}+1\rangle_{\{a\}acb}$	$2S-1$	1	$-(2S-2)$	0

We finish this section with the excited states corresponding to the multiplet $|\mathrm{GS}-1\rangle$, characterized by one less conduction electron than in the ground state. They transform as $[2S-1,1^{N-1}]$, and the highest weight state is

$$|\mathrm{GS}-1\rangle=\frac{1}{\sqrt{(2S-1)!}}(b_a^\dagger)^{2S-1}|\Delta'\rangle$$

with

$$|\Delta'\rangle\equiv\frac{1}{\gamma'}\mathcal{A}\left[b^\dagger_{i_1}\left(\prod_{\alpha=i_2}^{i_q}f^\dagger_\alpha\right)\left(\prod_{\beta=i_{q+1}}^{i_{N-1}}c^\dagger_\beta\right)\right]|0\rangle,$$

$$\gamma'\equiv\sqrt{(2S+N-2)C^{q-1}_{N-1}}.$$

Here, $|\Delta'\rangle$ transforms as the N-dimensional, $[1^{N-1}]$, representation of SU(N).

APPENDIX C: THE CASE OF THE ANTISYMMETRIC IMPURITY

The ground state for the strong-coupling fixed point of a Kondo model with a fermionic impurity (completely antisymmetric representation), $|\mathrm{GS}\rangle^{[1^N]}$, is a singlet formed with $(N-q)$ conduction electrons at site 0, and has the same form as $|\Delta\rangle$, in Eq. (6), but with a different normalization factor,

$$|\mathrm{GS}\rangle^{[1^N]}\equiv\frac{1}{\sqrt{C_N^q}}\mathcal{A}\left[\left(\prod_{\alpha=i_1}^{i_q}f^\dagger_\alpha\right)\left(\prod_{\beta=i_{q+1}}^{i_N}c^\dagger_\beta\right)\right]|0\rangle. \quad \text{(C1)}$$

The hopping Hamiltonian leads to two types of processes, as described earlier, where the intermediate states have either one more or one less conduction electron. With the help of Table I we can write the excitation energies

TABLE IV. Clebsch-Gordan coefficients for the process $[1]\otimes[2S-1]\to[2S]\oplus[2S-1,1]$. The label $|\{a\}aab\rangle$ indicates a state of $[2S]$, whereas $|\{a\}aa,b\rangle$ denotes the highest weight state in $[2S-1,1]$.

aab	N	$\|a\rangle\|\{a\}ab\rangle$	$\|b\rangle\|\{a\}aa\rangle$
$\|\{a\}aab\rangle$	$2S$	$2S-1$	1
$\|\{a\}aa,b\rangle$	$2S$	1	$-(2S-1)$

TABLE V. Same as Table IV, but for states with quantum numbers $(a)^{2S-2}bb$.

abb	N	$\|a\rangle\|\{a\}bb\rangle$	$\|b\rangle\|\{a\}ab\rangle$
$\|\{a\}abb\rangle$	$2S$	$2S-2$	2
$\|\{a\}ab,b\rangle$	$2S$	2	$-(2S-2)$

$$\Delta E_1=\frac{J}{2}\left(\frac{N+1}{N}\right)(N-q),\quad \Delta E_2=\frac{J}{2}\left(\frac{N+1}{N}\right)q.$$

It is clear that ΔE_1 and ΔE_2 are related by the *particle-hole* transformation $q\to(N-q)$.

The ground state with n_d electrons on site 1 is

$$|\mathrm{GS},n_d\rangle=(d_a^\dagger d_b^\dagger\cdots d_u^\dagger)|\mathrm{GS}\rangle.$$

Since there is only one intermediate state for each process, we can use the trick described in Sec. III C, and write

$$M_1=t^2\left(n_d-\sum_{\sigma,\sigma'}\langle\mathrm{GS},n_d|c_\sigma^\dagger d_{\sigma'}^\dagger d_\sigma c_{\sigma'}|\mathrm{GS},n_d\rangle\right). \quad \text{(C2)}$$

As long as $n_d>1$, the second term in Eq. (C2) vanishes for $\sigma\neq\sigma'$. c_σ acting on $|\mathrm{GS},n_d\rangle$ just counts the number of terms where there is a $c_\sigma^\dagger$. There are C_{N-1}^q such terms. Thus,

$$\sum_{\sigma,\sigma'}\langle\mathrm{GS},n_d|c_\sigma^\dagger d_{\sigma'}^\dagger d_\sigma c_{\sigma'}|\mathrm{GS},n_d\rangle=n_d\left(\frac{C_{N-1}^q}{C_N^q}\right)=n_d\left(\frac{N-q}{N}\right)$$

and

$$M_1=t^2 n_d\frac{q}{N}.$$

Finally, following Eq. (18),

$$M_2=t^2(n_c-n_d)+M_1=t^2(N-n_d)\left(\frac{N-q}{N}\right).$$

M_1 and M_2 are related by the same transformations ($q\to N-q$, $n_d\to N-n_d$) as the excitation energies. That means that the energy shift is invariant under these transformations

TABLE VI. Same as Table IV, but for states with quantum numbers $(a)^{2S-2}bc$. Notice the degeneracy in $[2S-1,1]$. We denote corresponding orthogonal states by $|\{a\}ab,c\rangle$ and $|\{a\}ac,b\rangle$.

abc	N	$\|a\rangle\|\{a\}bc]$	$\|b\rangle\|\{a\}ac\rangle$	$\|c\rangle\|\{a\}ab\rangle$
$\|\{a\}abc\rangle$	$2S$	$2S-2$	1	1
$\|\{a\}ab,c\rangle$	$2S(2S-1)$	$2S-2$	1	$-(2S-1)^2$
$\|\{a\}ac,b\rangle$	$2S-1$	1	$-(2S-2)$	0

$$\Delta E_f=-\left(\frac{2t^2}{J}\right)\left[\frac{n_d}{N+1}\left(\frac{q}{N-q}\right)+\frac{N-n_d}{N+1}\left(\frac{N-q}{q}\right)\right].$$

In the large-N limit, this result is equivalent to Eq. (22). To leading order in $1/N$, the energy shift of the strong-coupling fixed point is determined by the fermionic component, and the behavior under the particle-hole transformation.

APPENDIX D: DETAILS OF THE CALCULATIONS OF THE MATRIX ELEMENTS

Here we construct explicitely the excited states that are involved in the second-order perturbation theory, and then we compare them to the action of the hopping term, $(c_\sigma^\dagger d_\sigma)$, on the ground state. First, we add a c electron to the ground state, and then we combine it with (n_d-1) electrons from site 1.

1. Symmetric process: $|\mathrm{GS},n_d\rangle^S$

The strong-coupling excited state $|\mathrm{GS}+1\rangle^S$ is easy to compute, since it is the highest weight state in the product $[2S-1]\otimes[1]\to[2S]\oplus[2S-1,1]$. We have

$$|\mathrm{GS}+1\rangle_{aaa}^S=\frac{1}{\Omega}c_a^\dagger|\mathrm{GS}\rangle_{aa}$$

with the normalization factor $\Omega^2=(2S+q-1)/(2S+N-1)$. Other states within the same representation, which transform as $[2S]$, can be obtained by acting with the corresponding lowering operators. For instance,

$$|\mathrm{GS}+1\rangle_{aab}^S=\frac{1}{\Omega\sqrt{2S}}(\sqrt{2S-1}\;c^\dagger|\mathrm{GS}\rangle_{ab}+c_b^\dagger|\mathrm{GS}\rangle_{aa}).$$

TABLE VII. Some of the CG coefficients for the product of $k=n_d$ electrons, and an effective impurity $[2S-1]$, $([1^k]\otimes[2S-1]\to[2S,1^{k-1}]\oplus[2S-1,1^k]\oplus\cdots)$. Here we only keep the coefficients for the representations $[2S,1^{k-1}]$ and $[2S-1,1^k]$ (last row). States from $[1^k]$ are denoted by a column of labels, $|\vdots\rangle$; those from $[2S-1]$ are denoted $|\alpha\rangle$, and are states *close* to the highest weight state, denoted $|a\rangle$. The states in $[2S,1^{k-1}]$ are labeled $|ab,c,d,\ldots\rangle$ and those in $[2S-1,1^k]$, $|a,b,c,\cdots\rangle$.

$[1^k]\otimes[2S-1]$	N	$[1^k]\{\|\vdots\rangle\ \overbrace{\|a\rangle}^{[2S-1]}$	$\|\vdots\rangle\|b\rangle$	$\|\vdots\rangle\|c\rangle$	$\cdots$	$\|\vdots\rangle\|u\rangle$	$\|\vdots\rangle\|v\rangle$
$\{a\}abc,\ldots,uv$							
$\|ab,c,\ldots,u,v\rangle$	$2S(2S-1)$	$2S-1$	$(2S-1)^2$	0	$\cdots$	0	0
$\|ac,b,\ldots,u,v\rangle$	$2S(2S+1)$	$-(2S-1)$	1	$(2S)^2$	$\cdots$	0	0
$\cdots$		$\cdots$	$\cdots$	$\cdots$	$\cdots$	$\cdots$	$\cdots$
$\|au,b,\ldots,t,v\rangle$	$(2S+k-2)(2S+k-3)$	$(-1)^k(2S-1)$	$-(-1)^k$	$(-1)^k$	$\cdots$	$(2S+k-3)^2$	0
$\|av,b,\ldots,t,u\rangle$	$(2S+k-1)(2S+k-2)$	$(-1)^{k+1}(2S-1)$	$-(-1)^{k+1}$	$(-1)^{k+1}$	$\cdots$	1	$(2S+k-2)^2$
$\|a,b,\ldots,u,v\rangle$	$(2S+k-1)$	$(2S-1)$	-1	1	$\cdots$	$(-1)^{k-1}$	$(-1)^k$

The highest weight state of the antisymmetric multiplet $|\mathrm{GS}+1\rangle^A$, which transforms as $[2S-1,1]$, is a state orthogonal to $|\mathrm{GS}+1\rangle^S_{aab}$, that is,

$$|\mathrm{GS}+1\rangle^A_{aab}=\frac{1}{\Lambda\sqrt{2S}}(c^\dagger_a|\mathrm{GS}\rangle_{ab}-\sqrt{2S-1}\ c^\dagger_b|\mathrm{GS}\rangle_{aa})$$

with a different normalization factor, $\Lambda^2=(q-1)/(N-1)$. Other states can be obtained from these three. The results are summarized in Tables IV–VI of Clebsch-Gordan coefficients.

Next, we have to add the (n_d-1) electrons on site 1. The results of the calculations are summarized in Table VII. We have

$$|\mathrm{GS}+1,n_d-1\rangle^S_{aab\cdots u}=\frac{1}{\sqrt{2S+n_d-1}}\left[\sqrt{2S}\ \left(\prod_{i=2}^{n_d}d^\dagger_{x_i}\right)|\mathrm{GS}+1\rangle^S_{aaa}+\sum_{j=2}^{n_d}(-1)^{j-1}\left(\prod_{i=1,i\neq j}^{n_d}d^\dagger_{x_i}\right)|\mathrm{GS}+1\rangle^S_{aax_j}\right]$$

$$=\frac{1}{\Omega\sqrt{2S(2S+n_d-1)}}\left[2S\ \left(\prod_{i=2}^{n_d}d^\dagger_{x_i}\right)c^\dagger_a|\mathrm{GS}\rangle_{aa}\right.$$

$$\left.+\sum_{j=2}^{n_d}(-1)^{j-1}\left(\prod_{i=1,i\neq j}^{n_d}d^\dagger_{x_i}\right)(\sqrt{2S-1}\ c^\dagger_a|\mathrm{GS}\rangle_{ax_j}+c^\dagger_{x_j}|\mathrm{GS}\rangle_{aa})\right],$$

for the symmetric state in the symmetric configuration, and

$$|\overline{\mathrm{GS}+1,n_d-1}\rangle^S_{aab\cdots u}=\frac{1}{\sqrt{n_d-1}}\left[\sum_{j=2}^{n_d}(-1)^j\left(\prod_{i=1,i\neq j}^{n_d}d^\dagger_{x_i}\right)|\mathrm{GS}+1\rangle^A_{aax_j}\right]$$

$$=\frac{1}{\Lambda\sqrt{2S(n_d-1)}}\left[\sum_{j=2}^{n_d}(-1)^j\left(\prod_{i=1,i\neq j}^{n_d}d^\dagger_{x_i}\right)(c^\dagger_a|\mathrm{GS}\rangle_{ax_j}-\sqrt{2S-1}\ c^\dagger_{x_j}|\mathrm{GS}\rangle_{aa}\right),$$

for the antisymmetric state in the symmetric configuration $(x_1=a)$. From here, it is easy to show that the effect of $(c^\dagger_\sigma d_\sigma)$ on the ground state is given by Eq. (11).

2. Antisymmetric process: $|\mathrm{GS},n_d\rangle^A$

The action of $(c^\dagger_\sigma d_\sigma)$ on the ground state $|\mathrm{GS},n_d\rangle^A$, with n_d electrons on site 1 coupled antisymmetrically, produces

$$\left(\sum_\sigma c^\dagger_\sigma d_\sigma\right)|\mathrm{GS},n_d\rangle^A_{ab\cdots v}=\frac{(-1)^{n_d-1}}{\sqrt{2S+n_d-1}}\left[\sqrt{2S-1}\sum_{l=2}^{n_d+1}(-1)^l\left(\prod_{i=2,i\neq l}^{n_d+1}d^\dagger_i\right)c^\dagger_{x_l}|\mathrm{GS}\rangle_{aa}\right.$$

$$\left.+\sum_{j=2}^{n_d+1}(-1)^{j-1}\left\{\sum_{l=1}^{j-1}(-1)^{l-1}\left(\prod_{i=1,i\neq j,l}^{n_d+1}d^\dagger_i\right)+\sum_{l=j+1}^{n_d+1}(-1)^l\left(\prod_{i=1,i\neq j,l}^{n_d+1}d^\dagger_i\right)\right\}c^\dagger_{x_l}|\mathrm{GS}\rangle_{ax_j}\right],\tag{D1}$$

which is proportional to a given strong-coupling excited state. Since we can write Eq. (D1) as

$$\left(\sum_\sigma c^\dagger_\sigma d_\sigma\right)|\mathrm{GS},n_d\rangle^A_{ab\cdots v}=\frac{(-1)^{n_d-1}}{\sqrt{2S+n_d-1}}\left\{\sum_{l=2}^{n_d+1}(-1)^l\left(\prod_{i=2,i\neq l}^{n_d+1}d^\dagger_{x_i}\right)(\sqrt{2S-1}\ c^\dagger_{x_l}|\mathrm{GS}\rangle_{aa}-c^\dagger_a|\mathrm{GS}\rangle_{ax_l}\right)$$

$$+\sum_{j=2}^{n_d+1}(-1)^{j-1}\left[\sum_{l=2}^{j-1}(-1)^{l-1}\left(\prod_{i=1,i\neq j,l}^{n_d+1}d^\dagger_{x_i}\right)-\sum_{l=j+1}^{n_d+1}(-1)^{l-1}\left(\prod_{i=1,i\neq j,l}^{n_d+1}d^\dagger_{x_i}\right)\right]c^\dagger_{x_l}|\mathrm{GS}\rangle_{ax_j}$$

after some algebra, we get

$$\left(\sum_\sigma c_\sigma^\dagger d_\sigma\right)|\mathrm{GS},n_d\rangle^A_{ab\cdots v}=\frac{(-1)^{n_d-1}}{\sqrt{2S+n_d-1}}\sum_{l=2}^{n_d+1}(-1)^l\left\{\left(\prod_{i=2,i\neq l}^{n_d+1}d^\dagger_{x_i}\right)(\sqrt{2S-1}c^\dagger_{x_l}|\mathrm{GS}\rangle_{aa}-c^\dagger_a|\mathrm{GS}\rangle_{ax_l}\right)$$
$$-\sum_{j=2}^{l-1}(-1)^j\left(\prod_{i=1,i\neq j,l}^{n_d+1}d^\dagger_{x_i}\right)(c^\dagger_{x_l}|\mathrm{GS}\rangle_{ax_j}-c^\dagger_{x_j}|\mathrm{GS}\rangle_{ax_l}).$$

This expression can be written using the antisymmetric states $|\mathrm{GS}+1\rangle^A$, with the help of the following relations:

$$\Lambda(\sqrt{2S}\ |\mathrm{GS}+1\rangle^A_{ax_lx_j}-\sqrt{2S-2}\ |\mathrm{GS}+1\rangle^A_{ax_jx_l})=\sqrt{2S-1}(c^\dagger_{x_l}|\mathrm{GS}\rangle_{ax_j}-c^\dagger_{x_j}|\mathrm{GS}\rangle_{ax_l}),$$

$$\Lambda\sqrt{2S}\ |\mathrm{GS}+1\rangle^A_{aax_l}=c^\dagger_a|\mathrm{GS}\rangle_{ax_l}-\sqrt{2S-1}\ c^\dagger_{x_l}|\mathrm{GS}\rangle_{aa},$$

to obtain

$$\left(\sum_\sigma c_\sigma^\dagger d_\sigma\right)|\mathrm{GS},n_d\rangle^A_{ab\cdots v}=\frac{(-1)^{n_d-1}\Lambda}{\sqrt{(2S+n_d-1)(2S-1)}}\sum_{l=1}^{n_d+1}(-1)^{l+1}\left\{\left(\prod_{i=2,i\neq l}^{n_d+1}d^\dagger_{x_i}\right)\sqrt{2S(2S-1)}\ |\mathrm{GS}+1\rangle^A_{aax_l}\right.$$
$$\left.-\sum_{j=2}^{l-1}(-1)^j\left(\prod_{i=1,i\neq j,l}^{n_d+1}d^\dagger_{x_i}\right)(\sqrt{2S}\ |\mathrm{GS}+1\rangle^A_{ax_jx_l}-\sqrt{2S-2}\ |\mathrm{GS}+1\rangle^A_{ax_lx_j})\right.$$

Finally, since

$$\left(\sum_\sigma c_\sigma^\dagger d_\sigma\right)|\mathrm{GS},n_d\rangle^A_{ab\cdots v}\propto|\mathrm{GS}+1,n_d-1\rangle^A_{ab\cdots v},\tag{D2}$$

we just have to normalize the previous state in order to obtain the excited state $|\mathrm{GS}+1,n_d-1\rangle^A_{ab\cdots v}$. Up to a sign, we have

$$|\mathrm{GS}+1,n_d-1\rangle^A_{ab\cdots v}=\frac{1}{\sqrt{n_d(2S+n_d-1)(2S-1)}}\sum_{l=1}^{n_d+1}(-1)^{l+1}\left\{\left(\prod_{i=2,i\neq l}^{n_d+1}d^\dagger_{x_i}\right)\sqrt{2S(2S-1)}\ |\mathrm{GS}+1\rangle^A_{aax_l}\right.$$
$$\left.-\sum_{j=2}^{l-1}(-1)^j\left(\prod_{i=1,i\neq j,l}^{n_d+1}d^\dagger_{x_i}\right)(\sqrt{2S}\ |\mathrm{GS}+1\rangle^A_{ax_jx_l}-\sqrt{2S-2}\ |\mathrm{GS}+1\rangle^A_{ax_lx_j})\right.$$

and

$$\left(\sum_\sigma c_\sigma^\dagger d_\sigma\right)|\mathrm{GS},n_d\rangle^A_{ab\cdots v}=(\Lambda\sqrt{n_d})|\mathrm{GS}+1,n_d-1\rangle^A_{ab\cdots v}.$$

3. Tables of Clebsch-Gordan coefficients

The calculation of the excited states involves the use of some Clebsch-Gordon coefficients. We have evaluated these quantities explicitely for arbitrary $2S$, n_d, and N, following the steps outlined in Appendix B1. We summarize our results in Tables IV–VII. In the tables, all the coefficients are assumed to be under the sign of the square root. For instance, $-(2S-1)$ corresponds to $-\sqrt{2S-1}$. The states should be divided by the normalization factor $\sqrt{N}$. Tables IV–VI are required when one electron is added to the effective impurity, $([1]\otimes[2S-1])$. Table VII corresponds to the addition of n_d electrons.

*Also at the Centre National de la Recherche Scientifique (CNRS).

[1] S. Sachdev, *Quantum Phase Transitions* (Cambridge University Press, Cambridge, 1999).
[2] G. Stewart, Rev. Mod. Phys. **73**, 797 (2001).
[3] H.v. Löhneysen, A. Schröder, M. Sieck, and T. Trappmann, Phys. Rev. Lett. **72**, 3262 (1994).
[4] H.v. Löhneysen, J. Phys.: Condens. Matter **8**, 9689 (1996).
[5] S. Kambe, S. Raymond, L. Regnault, J. Flouquet, P. Lejay, and P. Haen, J. Phys. Soc. Jpn. **65**, 3294 (1996).
[6] O. Trovarelli, C. Geibel, S. Mederle, C. Langhammer, F.M. Grosche, P. Gegenwart, M. Lang, G. Sparn, and F. Steglich, Phys. Rev. Lett. **85**, 626 (2000).
[7] F. Steglich *et al.*, Z. Phys. B: Condens. Matter **103**, 235 (1997).
[8] F. Steglich *et al.*, J. Phys.: Condens. Matter **8**, 9909 (1996).
[9] N. Mathur, F. Grosche, S. Julian, I. Walker, D. Freye, R. Haselwimmer, and G. Lonzarich, Nature (London) **394**, 39 (1998).
[10] C. Seaman, M. Maple, B. Lee, S. Ghamaty, M. Torikachvili, J.-S. Kang, L. Liu, J. Allen, and D. Cox, Phys. Rev. Lett. **67**, 2882 (1991).
[11] J. Hertz, Phys. Rev. B **14**, 1165 (1976).

[12] A. Millis, Phys. Rev. B **48**, 7183 (1993).
[13] M. Continentino, Phys. Rev. B **47**, 11 581 (1993).
[14] T. Moriya and T. Takimoto, J. Phys. Soc. Jpn. **64**, 960 (1995).
[15] M. Lavagna and C. Pépin, Phys. Rev. B **62**, 6450 (2000).
[16] A. Schröder, G. Aeppli, E. Bucher, R. Ramazashvili, and P. Coleman, Phys. Rev. Lett. **80**, 5623 (1998).
[17] A. Schröder, G. Aeppli, R. Coldea, M. Adams, O. Stockert, H. Löhneysen, E. Bucher, R. Ramazashvili, and P. Coleman, Nature (London) **407**, 351 (2000).
[18] P. Coleman, Physica B **259-261**, 353 (1999).
[19] Q. Si, S. Rabello, K. Ingersent, and J.L. Smith, Nature (London) **413**, 804 (2001).
[20] R. Bulla and M. Vojta, cond-mat/0210015.
[21] D. Withoff and E. Fradkin, Phys. Rev. Lett. **64**, 1835 (1990).
[22] K. Ingersent and Q. Si, Phys. Rev. Lett. **89**, 076403 (2002).
[23] M. Vojta and R. Bulla, Phys. Rev. B **65**, 014511 (2002).
[24] J. Gan, P. Coleman, and N. Andrei, Phys. Rev. Lett. **68**, 3476 (1992).
[25] C. Pépin and M. Lavagna, Phys. Rev. B **19**, 12 180 (1999).
[26] P. Coleman, C. Pépin, and A. Tsvelik, Phys. Rev. B **62**, 3852 (2000).
[27] P. Coleman, C. Pépin, and A.M. Tsvelik, Nucl. Phys. B **586**, 641 (2000).
[28] P. Anderson, J. Phys. C **3**, 2436 (1970).
[29] P. Nozières, J. Phys. (Paris) **37**, C1 (1976).
[30] A. Hewson, *The Kondo Problem to Heavy Fermions* (Cambridge University Press, Cambridge, 1993).
[31] P. Nozières and A. Blandin, J. Phys. (Paris) **41**, 193 (1980).
[32] N. Andrei and C. Destri, Phys. Rev. Lett. **52**, 364 (1984).
[33] A.M. Tsvelik and P.B. Wiegman, Z. Phys. B **54**, 201 (1984).
[34] D.L. Cox and A.E. Ruckenstein, Phys. Rev. Lett. **71**, 1613 (1993).
[35] M. Hammermesh, *Group Theory and its Application to Physical Problems* (Addison-Wesley, Reading, MA, 1962).
[36] H. Jones, *Group Representations and Physics* (Institute of Physics, University of Reading, Berkshire, 1990).
[37] J. Cornwell, *Group Theory in Physics* (Academic, London, 1986).
[38] D. Lichtenberg, *Unitary Symmetry and Elementary Particles* (Academic Press, New York, 1970).
[39] B. Coqblin and J.R. Schrieffer, Phys. Rev. **185**, 847 (1969).
[40] S. Okubo, J. Math. Phys. **18**, 2382 (1977).
[41] O. Parcollet, A. Georges, G. Kotliar, and A. Sengupta, Phys. Rev. B **58**, 3794 (1998).
[42] A. Jerez, N. Andrei, and G. Zaránd, Phys. Rev. B **58**, 3814 (1998).
[43] I. Affleck and A.W.W. Ludwig, Phys. Rev. B **48**, 7297 (1993).
[44] N. Andrei (private communication).
[45] P. Kulish, N.Y. Reshetikhin, and E.K. Sklyanin, Lett. Math. Phys. **5**, 393 (1981).
[46] D. Arovas and A. Auerbach, Phys. Rev. B **38**, 316 (1988).
[47] A. Abrikosov, Physics (Long Island City, N.Y.) **2**, 5 (1965).
[48] I.V. Schensted, *A Course on the Application of Group Theory to Quantum Mechanics* (NEO Press, Maine, 1976).
[49] J. Chen, P. Wang, Z. Lü, and X. Wu, *Tables of the Clebsch-Gordan, Racah, and Subduction Coefficients of SU(n) Groups* (World Scientific, Singapore, 1987).